# Ultrasonic Doppler Measurement of Renal Artery Blood Flow

by

William R. Freund
James D. Meindl

August 1975

Progress Report (March 1, 1974-August 31, 1975)

Prepared under

National Aeronautics and
Space Administration
Grant NGR-05-020-615



INTEGRATED CIRCUITS LABORATORY

STANFORD ELECTRONICS LABORATORIES

STANFORD UNIVERSITY · STANFORD, CALIFORNIA

SEL-76-004

Progress Report to
The National Aeronautics and Space Administration
for the Period
March 1, 1974 - August 31, 1975

Ames Research Center
Moffett Field, California 94305

# ULTRASONIC DOPPLER MEASUREMENT OF RENAL ARTERY BLOOD FLOW

by

William R. Freund and James D. Meindl

Grant Number NGR-05-020-615
Technical Report 4962-2

Submitted by
The Integrated Circuits Laboratory
Stanford Electronics Laboratories
Stanford University, California
August 1975

## Abstract

This progress report summarizes research completed during the past three semi-annual periods, March 1, 1974 through August 31, 1975. This work provides an extensive evaluation of the practical and theoretical limitations encountered in the use of totally implantable CW Doppler flowmeters. Theoretical analyses, computer models, *in-vitro* and *in-vivo* calibration studies describe the sources and magnitudes of potential errors in the measurement of blood flow through both the renal artery, and larger vessels in the circulatory system. The evaluation of new flowmeter/transducer systems and their use in physiological investigations is reported.

TABLE OF CONTENTS

Table of Contents

## Introduction

The development of totally implantable Doppler flowmeters for the measurement of renal blood flow has been previously reported [1,2,3]. The purpose of research completed during the last 18 months has been to provide an extensive evaluation of the theoretical and practical limitations encountered in the use of these systems. Such evaluations serve four major purposes: (1) They guide NASA personnel in specifying instrumentation for future animal flight experiments, (2) they assist potential users in determining the applicability of the CW Doppler technique for their experimental protocols, (3) they critique our own development efforts to date, and (4) they may signal areas where improvements in commercially available flowmeters are required. The accomplishments towards this goal fall into four broad categories:

(1) Theoretical Evaluations
(2) In-Vitro Evaluations
(3) Acute In-Vivo Evaluations
(4) Chronic In-Vivo Evaluations

Specifically, the accomplishments include:

(1) The theoretical analysis of potential error sources and their relative magnitudes for a current CW flowmeter design.

(2) The initiation of in-vitro calibration studies with this flowmeter design for comparison with the results from task (1).

(3) The completion of an experiment to characterize the acoustic properties of canine descending aorta.

(4) The initiation and partial completion of an in-vivo acute calibration protocol to:

  (a) identify the actual error sources encountered, and

  (b) compare the magnitudes of these errors with theoretically predicted values.

(5) The development of real-time spectral analysis as a research tool to provide evaluations of "zero crosser" performance and add a new output mode for existing systems.

(6) The chronic implantation of eleven flowmeter and transducer systems and their subsequent use in a variety of physiological studies involving renal, iliac, and mesenteric blood velocities during rest, exercise, and lower body negative pressure.

(7) The evaluation of a chronically implanted integrated circuit CW directional flowmeter. This was accomplished by comparing simultaneous waveforms produced by the totally implanted CW system, and an adjacent EMF flowmeter cuff which used percutaneous leads.

(8) The development and implanted evaluation of a special purpose transducer to measure velocities and velocity profiles adjacent to the mitral and tricuspid valves.

(9) The investigation of techniques to allow more efficient collection and analysis of telemetered physiological data.

As with all the in-vivo studies, the work in task #9 was completed in collaboration with research personnel at Ames Research Center, Moffett Field, California. An abstract of this work will be included.

# THEORETICAL ERROR ANALYSIS FOR PERIVASCULAR DOPPLER FLOW TRANSDUCERS

## 1.1 Introduction to Error Analysis

CW Doppler techniques have been used by medical investigators for almost two decades. During this period numerous authors have described various theoretical and practical aspects of the Doppler process. (See for example references 4 - 7). Despite this experience, there is little published information describing the sources and magnitudes of errors encountered in the use of implantable CW Doppler transducers. Consequently, many researchers continue to rely on electromagnetic techniques for the measurement of pulsatile blood flow.

This theoretical analysis identifies and quantifies the errors in the use of totally implantable CW Doppler transducers. The predicted errors are validated by in-vitro and in-vivo studies. Initial results are presented in Section IV.

The uncertainty for velocity and flow estimates is a function of:

(1) The size of the piezoelectric element relative to the vessel lumen,

(2) The construction and symmetry of the transducer cuff,

(3) The acoustical and mechanical coupling to the vessel,

(4) Flow hemodynamics,

(5) The statistical performance of common zero-crossing detectors, and

(6) The technique for estimating the vessel lumen area.

Topic (5) will be considered in Section 1.2 and 1.5.

## 1.2 The Relative Size of the Piezoelectric Elements

The relative size of the piezoelectric elements has profound effects on the accuracy of velocity and volume flow estimation using Doppler techniques. When choosing a transducer for a specific vessel size and target parameter, one should consider the impact of element size on: (1) signal-to-noise ratio (2) the relationship between velocities in the sample volume and the average velocity across the vessel, and (3) signal processing errors due to spreading of the Doppler spectrum.

Figure 1.1 shows the familiar symmetrical arrangement of the transmitting and receiving transducers on either side of the vessel. It is easily appreciated that (for near field operation of ideal transducers) as the transducers become arbitrarily small, so will the dimensions of the sample volume. In the limit, all the particles within the sample volume will approach the same velocity, producing a line Doppler spectrum. For signal-to-noise ratios in excess of 20 dB a zero-crossing processor will produce a perfect estimation of the mean frequency within that spectrum. Conversely, as the transducers become arbitrarily large (whole vessel illumination), the particles within the sample are more likely to contain a wide range of velocities. The Doppler spectrum will then be determined by the instantaneous velocity profile across the vessel. For a frequency spectrum produced by a parabolic profile, theory predicts that zero crossing demodulators will overestimate the mean frequency by 15%. In

practice, however, it is difficult to achieve perfectly uniform illumination. Additionally, the theory developed by Rice [8] applies only to true zero-crossing meters which have no hysteresis or bandpass filtering. Empirically, the addition of hysteresis reduces the magnitude of this error.

In practice, the piezoelectric materials can be neither arbitrarily small nor large without encountering serious theoretical, construction or application difficulties. The expected errors for transducers in this intermediate range are not easily calculated. This is partially due to the complex interactions between sample volumes with cartesian symmetry and velocity profiles which typically have radial symmetry. Fortunately, such interactions can be analyzed via computer models and the results will be presented in a later section.

Signal-to Noise Ratio

Flax, Brody, DiPietro and Frescura have considered the implications of altering the size of the piezoelectric elements with respect to the vessel inner diameter [9 - 12]. DiPietro derived a transfer function describing the ratio between the transmitted and received ultrasonic power as a function of piezoelectric element size, drive frequency, transducer angle, red cell concentration, ultrasonic attenuation and the lumen diameter [11]. He found that for square elements and with all other variables held constant, the backscattered power would increase as the transducer edge length cubed. For example, increasing the transducer element size from .1 (vessel inner diameter) to .5 (vessel inner diameter)

would increase backscattered power in excess of 20 dB. This would increase the audio signal-to-noise ratio as long as the sample volume remained completely within the vessel lumen. When the sample volume intersects the vessel walls, large echoes from the wall may become part of the Doppler spectrum. If the walls are moving, the net result is the addition of high amplitude, low frequency signals which must be removed for accurate estimation of blood velocity. This problem will be most pronounced during acute experiments, where there is no fibrous scar tissue to secure the cuffs. Practically, the maximum audio signal-to-noise ratio is limited by the spectral purity of the ultrasonic oscillator and the noise figures of the signal processing stages.

Properties of the Sample Volume and Impact on Measurement Accuracy

We must now consider other implications of altering the size of the piezoelectric elements. Specifically:

(1) What are the dimensions of the sample volume as a function of element size and angle?

(2) What is the mean velocity within the sample volume and how does it relate to the mean velocity across the vessel?

(3) How accurately will a zero-crossing detector estimate the mean velocity within a given sample volume?

(4) Finally, how do these factors combine to produce discrepancies between the flowmeter output and the mean velocity within the vessel?

Computer Model

In order to answer these questions, a computer model has been formulated with the following simplifying assumptions:

(1) The interactions between the incident ultrasound and moving blood can be modeled as a first order scattering process. [13]

(2) The scatterers have a homogeneous distribution within the sample volume.

(3) The radial velocity of particles within the sample volume is equal to zero.

(4) The transducers are ideal and operating in the near field.

(5) Spectral spreading due to diffusion and transit time through the sample volume can be ignored.

(6) The transducer beam pattern remains unchanged as it passes through the vessel wall.

(7) The effects of the attenuation of the ultrasonic energy as it traverses the vessel will be offset by the symmetric placement of the transducer crystals.

As shown in Figure 1.2, the sample volume is the product of the beam patterns for the two piezoelectric elements. The projection of the sample volume onto the Cartesian x-z plane is a function of the element height, d, and the angle of intersection between the ultrasonic beams and the z-axis ($\theta$). The maximum x excursion is $d/\cos\theta$, while the maximum z excursion is $d/\sin\theta$. The projection of the sample volume in the yz plane is simply the element width w. Note that with ideal transducer placement, the sample volume possesses perfect Cartesian symmetry.

Recall from our assumption of first order scattering that back

scattered power is directly proportional to the number of scatterers in the sample volume. In order to express the backscattered power as a function of location in the x-y plane one must then know the corresponding z excursion of the sample volume ($\Delta z$) and the particle density at that point ($\rho$). The number of scatterers ($N_{xy}$) then equals $\rho_{xy}\Delta z_{xy}$. If we assume a homogeneous particle distribution, $N_{xy}$ is a linear function of $\Delta z_{xy}$. One can then define a geometric space where $z_{xy} = N_{xy}$ for all values of x and y within a particular vessel cross section. In other words, the backscattered power corresponding to any xy location is directly related to the height of the sample volume at that point on the xy plane.

In contrast to this, velocity profiles within the blood vessels are usually characterized as having radial symmetry, that is

$$V_r = V_{max}(1 - r^n) \qquad 1.1$$

where

$V_r$ = the velocity at some radial distance r from the center of the vessel

$V_{max}$ = the maximum (centerline) velocity

n = the profile number which typically varies from 2 to 12

A velocity space can then be defined by rotating this two-dimensional velocity profile about the center axis of the vessel.

Thus, each point in the xy plane maps onto two scaler fields specifying the velocity v(x,y) and the number of scatterers moving at that velocity, N(x,y). The mean velocity for all particles within

the sample volume is then:

$$\bar{V}_{s.v.} = \frac{\int v_{xy} \cdot N_{xy}\, dA}{\int N_{xy}\, dA} \qquad 1.2$$

where $N_{xy} = 0$ outside the sample volume.

Once calculated, the mean velocity within the sample volume can be compared with the mean velocity across the vessel. Where:

$$\bar{V}_{vessel} = \frac{\int v \cdot dA}{\int dA} = \frac{\int_0^1 (1 - r^n) 2\pi r\, dr}{\int_0^1 2\pi r\, dr} \qquad 1.3$$

Finally, it is known [14] that a zero crossing detector (without hysteresis) measures the RMS value of the frequency spectrum. Translated to velocities, this becomes:

$$\bar{v}_{zc} = \sqrt{\frac{\int v_{xy}^2 N_{xy} \cdot dA}{\int N_{xy} \cdot dA}} \qquad 1.4$$

where

$\bar{v}_{zc}$ = zero crossing estimate of mean velocity within the sample volume. This assumes for the moment, all other error sources are fixed and = 0.

One can then use computer models to compare $\bar{V}_{s.v.}$, $\bar{V}_{vessel}$ and $\bar{v}_{zc}$ for variations in element size and angle, and profile number, In addition, one could also model complex and asymmetric velocity profiles,

as well as spectral spreading due to diffusion and transit time through the sample volume.

Results of the Model

Figures 1.3 - 1.7 illustrate some of the comparisons described above. Figure 1.3 plots $\overline{V}_{s.v.}$ and its percent error from $\overline{V}_{vessel}$ as a function of transducer element size. These results are for square transducers for two different velocity profiles (n = 2 and 5). For a parabolic profile (at $\theta = 60^{0}$) the mean velocity within the sample volume will range from .98 to .54 $V^{*}_{max}$ for practical transducer sizes. Note that even when the edge length of the element equals the inner diameter of the vessel, the $\overline{V}_{vessel}$ is overestimated by 8%. This error is due to the geometry of the sample volume and entirely independent of the Doppler processing scheme employed.

Figure 1.4 shows similar plots for rectangular transducers for three different profiles (n = 2, 5 and 12). Note that the mean velocity within the sample volume ($\overline{V}_{sv}$) falls more slowly and uniformly than for square transducers.

Analysis of Eq.(1.4) indicates an overestimation of the mean frequency as the Doppler spectrum broadens. Figure 1.5 shows the zero-crossing overestimation of the mean velocity within the sample volume as a function of transducer size and geometry, and profile number.

$$\% \text{ error} = \frac{\overline{V}_{zc} - \overline{V}_{sv}}{\overline{V}_{sv}} \times 100 \qquad 1.5$$

Note that this error remains less than 6% until the transducer element size approaches the inner diameter of the vessel.

---

* Recall that $V_{max}$ = maximum (centerline) velocity

The curves in Figure 1.6 were generated by holding transducer size constant and allowing the profile number to vary. They indicate the range of errors or uncertainty in velocity measurement if the velocity profile varies during the cardiac cycle.

Figure 1.7 combines all of these factors to express the uncertainty in the zero-crossing estimate of the mean velocity across the vessel as a function of transducer size.

$$\gamma = \frac{\overline{V}_{zc} - \overline{V}_{vessel}}{\overline{V}_{vessel}} \times 100 \qquad 1.6$$

The percent errors are plotted for two different velocity profiles and for two different transducer geometries. It should be restated, however, that these results are based on computer models for ideal transducers and zero-crossing detectors without hysteresis or bandpass. These results will be confirmed by in-vitro and in-vivo studies.

Additionally, these analyses ignored any large reflections from fixed or moving vessel walls and assumed radially symmetric velocity profiles of the form $V_{(r)} = V_{max}(1 - r^n)$. This type of symmetry does not always exist, especially in large arteries near the heart [15]. Gerzberg and Meindl [16] have shown that for Doppler signals with simultaneous forward and reverse components, the components must be weighted by their relative power levels to correctly estimate net flow velocity. Commercially available flowmeters [17] do not employ this technique. The practical implications of these results will be considered in Section 1.5.

## 1.3 The Construction and Symmetry of the Transducer Cuff

Once the element size has been optimized for a particular lumen and target parameter, the following questions must be considered:

(1) What is the effect of errors in angle (during assembly) on the accuracy of velocity and flow measurements?

(2) What are the effects of axial offset during implantation of the two halves of the transducer shells?

(3) What are the effects of angular offset either due to manufacturing errors or incomplete closure of the cuff around the vessel?

The accuracy of velocity estimation with commercially available Doppler systems is dependent on knowledge of the relative angles between the ultrasonic beam and the blood velocity vectors ($\theta$). For the equation

$$\Delta f = V_b \, k \cos\theta \qquad 1.7$$

where $\Delta f$ = Doppler shift

$V_b$ = blood velocity

$k$ = constant

the sensitivity with respect to $\theta$ is

$$S_\theta = - V_b \, k \sin\theta \qquad 1.8$$

This implies, therefore, that $\Theta$ should be small for minimum angle dependence. In practice, however, $\theta$ will probably be $45^{o}$ or larger due to near field constraints and the desirability of keeping the sample volume within the portion of the vessel constrained by the cuff. At $\theta = 60^{o}$, a one degree angle error produces a 3% error in velocity estimation.

Cuff Symmetry

Assuming all cuffs are constructed of inflexible materials, at least two error sources may exist:

(1) Axial Offset

As shown in Figure 1.8, misalignment of the two cuff halves during assembly or implantation will shift the sample volume away from the vessel center. This produces the greatest errors with center vessel illumination and parabolic velocity profiles. An axial misalignment of 10% of the cuff diameter will shift the center of the sample volume by .125 x (cuff diameter). Assuming a 15% vessel wall thickness, this is equivalent to 15% of the vessel inner diameter. As shown in Figure 1.9a, this will decrease the velocity at the center of the sample volume by 10%.

(2) Angular Offset

Angular offset can occur either due to manufacturing errors or incomplete closure of the cuff around the vessel. As shown in Figure 1.9b, the net effect is to move the sample volume along the line formed by the mating surfaces of the cuff halves.

$$\text{Distance moved} = \frac{d}{2} \sin \phi \qquad 1.9$$

where $d$ = cuff diameter

$\phi$ = angular offset in degrees

An $11^{o}$ offset shifts the center of the sample volume by 10% of the cuff diameter. The same comments concerning relative sizes between transducer and vessel diameter apply as in axial offset (#1)

In summary, these errors can be virtually eliminated by use of locking alignment pins in the half shells, by use of a single piece shell, or by careful placement of the cuff on the vessel.

## 1.4 The Acoustical and Mechanical Coupling to the Vessel

Assuming all questions about cuff symmetry have been answered, the user must then consider the mechanics of fitting the flow cuff to the vessel.

### Coupling Materials

Various materials have been used to couple ultrasonic energy between the piezoelectric elements and the vessel wall. These include commercially available water based gels, sterile auger, epoxy and clotted blood. Each of these materials may have advantages in a particular application. The important point to remember is that ultrasonic energy obeys Snell's law of refraction (Figure 1.10).

By Snell's law

$$\frac{\sin \gamma_1}{\sin \gamma_2} = \frac{c_1}{c_2} \qquad 1.10$$

where $c_1$ = velocity of ultrasound in material 1

$c_2$ = velocity of sound in material 2

That is, the angle between the incident ultrasound and direction of blood flow can be shifted if the propagation velocity for the coupling material is different from that of blood. For example, if water is used as a coupling medium and $\gamma_1 = 30$, then $\gamma_2 = 32^{o}$. Velocity would then be overestimated by approximately 6% if the effects of refraction are ignored.

Probe Fit

In order to obtain dependable flow signals, one must carefully match the inner diameter of the cuff to the outer diameter of the vessel. For acute studies, many researchers prefer a cuff which constricts the blood vessel by approximately 10%. This helps to insure acoustical coupling between the elements and vessel walls, and minimizes the high amplitude low frequency wall motion signals which may create significant errors in flow velocity estimations. If the probe is too tight, however, both the hydraulic impedance of the blood vessel and flow waveform may be altered significantly.

In contrast, chronically implanted transducers should not constrict the vessel. Coupling and wall motion problems are minimized by rapid scarring which secures the transducers in place. Various linings can be used to minimize abrasion and promote fibrous scar tissue growth. The user should also consider the possiblity that the exposed vessel has changed size due to active vasoconstriction or changes in transmural pressure and may return to its original size following the surgical procedure.

Cuff Canting on Vessel

Cuff canting on the vessel is equivalent to rotating a fixed triangle about one end (Figure 1.11a). For a given angular rotation $\Omega$, the sample volume coordinates become:

$$x = (.58\ d) \cos (30 + \Omega) \qquad 1.10$$

$$z = (.58\ d) \sin (30 + \Omega) \qquad 1.11$$

where d = inner diameter of cuff

$30^{o}$ = transducer angle

$\Omega$ = angular rotation about one of the acute angles

For the x coordinate, an angular rotation of $13^{o}$ produces a horizontal shift of .1 diameter (cuff i.d.). A rotation of $13^{o}$ also displaces the y coordinate by approximately .1 of the cuff i.d. The effects of such displacements have been discussed in Section 1.3.

In addition to shifting the coordinates of the center of the sample volume, canting also affects the accuracy of axial velocity estimation for flows within the sample volume (Figure 11b ) This is true because the CW technique measures velocity components along the axis of the cuff. Thus flow velocities are underestimated by (1 - cos $\Omega$). Canting the cuff by $25^{o}$ produces a 10% error in axial velocity estimation.

Focusing Due to Vessel Wall Curvature

As illustrated below, the ultrasonic beam suffers a slight dispersion as it passes through the concentric curvatures of the vessel wall. This de-focusing is most pronounced when:

(1) The vessel wall thickness is large with respect to the vessel o.d.

(2) The transducer size approaches the vessel outer diameter, and

(3) There is severe mismatch between the propagation velocities of ultrasound in blood and in the coupling material.

For example, assume the following conditions:

$$\text{wall thickness} = \frac{.15}{2} \times (\text{vessel o.d.}) = .075 \times (\text{vessel o.d.})$$

$$\text{transducer size} = .707 \times (\text{vessel o.d.})$$

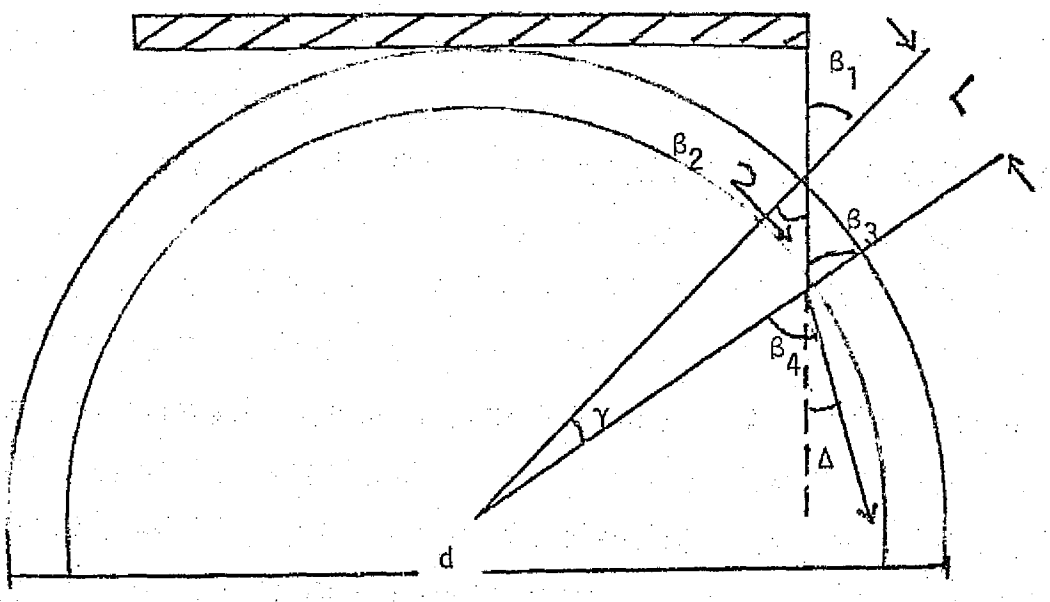


$$\beta_1 = 45^o \qquad \frac{\sin \beta_1}{\sin \beta_2} = \frac{c_1}{c_2} = \frac{1480}{1540} \; * \quad (* \text{ PNT Wells})$$

$$\beta_2 = \sin^{-1}(.736) = 47.5^o$$

$$\text{Chord length } L = (.075) \times (\tan \beta_2)$$

$$\gamma^o = \frac{L}{\pi d} \times 360 = \frac{.075 \times 1.09}{3.14} \times 360 = 9.4^o$$

$$\beta_3 = \beta_2 + \gamma = 47.5 + 9.4 = 56.9^o$$

$$\sin \beta_4 = \frac{c_3}{c_2} \sin \beta_3 = \frac{1570}{1540} \times .839 = .855$$

$$\beta_4 = \sin^{-1}(.855) = 59^o$$

The total beam dispersion would then be

$$\Delta = \beta_4 - \gamma - \beta_1 = 5^o \qquad 1.12$$

## 1.5 Flow Hemodynamics

Perivascular transducers can provide detailed information on the hemodynamics of vascular flow. Meaningful interpretations of these data, however, require consideration of the converse question. That is, how will hemodynamic variations affect the accuracy of velocity and volume flow estimates by CW techniques? Four questions will be considered in this Section:

(1) What waveform distortions are caused by velocity profile variations during the cardiac cycle?

(2) Can these errors be corrected by computation of Womersley's index of pulsatility, $\alpha$ [18]?

(3) What are the effects of turbulence on measurement accuracy?

(4) How do changes in hematocrit affect measurement accuracy?

### Waveform Distortion

As stated in Section 1.2, blood velocity profiles are often characterized as having radial symmetry of the form:

$$V_r = V_{max}(1 - r^n)$$

This formula is most applicable for steady, fully developed flow in non-distensible tubes. Womersley [18] was among the first of many researchers to solve the Navier-Stokes equations for the analysis of oscillatory blood flow in distensable tubes. His linear model predicted symmetries often quite different from the steady flow case.

Figure 1.12 shows the predicted, time varying profiles which can be calculated [19] with knowledge of pumping frequency, the inner diameter of the vessel, and the kinematic viscosity of blood. Time varying velocity profiles are shown for three values of $\alpha$ (dimensionless) where:

$$\alpha = R\sqrt{\frac{W}{\upsilon}}$$

R = vessel radius

W = pulsatile frequency

$\upsilon$ = kinematic viscosity of blood

As $\alpha$ increases so does the bluntness of the velocity profile during peak forward flow. For $\alpha = 2.5$, a sinusoidal driving function produces profiles which are nearly parabolic for much of the flow cycle. At $\alpha = 5.5$, the effects of fluid inertia are evident. Throughout the first $90^{o}$ of the cycle, there exists a region of high shear near the vessel wall with lower velocities in the center of the vessel. When $\alpha = 9.5$, the effects of inertia are clearly seen. The central core continually lags the flow of the wall shear region, keeping its blunt shape throughout the cardiac cycle. These predictions have been verified with in-vitro models by several investigators.

The in-vivo forcing function (ventricular pressure) is, however, much closer to a square wave than a sine wave. One must then consider the superposition of effects from both the fundamental and higher order

harmonic frequencies. The profiles in Figure 1.13 were calculated in this manner by McDonald [20] from measured pressure gradients in the femoral artery of a dog. Here, the profile number is seen to vary from 2 to 10 during the first $105^{0}$ of the cardiac cycle. Figure 1.6 showed that under these conditions, $\overline{V}_{s.v.}$ would be overestimated by less than 5% for all but the largest transducers. If however, the mean velocity across the vessel is desired, Figure 1.14 shows that $\overline{V}_{vessel}$ will be overestimated by variable amounts depending on the transducer size and profile number. For the case of d = .25 x (vessel i.d.), changing "n" from 3 to 10 decreases the % overestimation from 65% to 20%. Significant differences in waveform could then be expected in comparisons between EMF and Doppler flowmeters on the same vessel. These results would suggest that waveform distortion during early systole can be minimized by increasing transducer size. From $120^{0}$ to $270^{0}$, the center velocity in Figure 1.13 lags the mean velocity across the vessel. For small transducers this will tend to elongate the systolic waveform with respect to signals produced by adjacent EMF systems. Increasing the element size to illuminate the whole vessel creates a problem we must now confront.

Many commercial flowmeters employ a power splitting technique to produce bi-directional signals. The spectra corresponding to positive and negative flows are separated and passed simultaneously through separate zero-crossing detectors. They are then subtracted without any normalization for the relative power levels (i.e., number of scatterers) involved. Gerzberg and Meindl have shown [16] that with this method

a small number of scatterers moving in one direction can completely cancel the contributions from a much greater number of scatters moving in the opposite direction. This creates the potential for significant errors in both magnitude and direction throughout much of the cardiac cycle. Replacement of the zero-crossing detectors by single sideband first moment processors will not correct errors of this type, unless power normalization is also added.

The directional Doppler systems tested during the past contract year employ a different power splitting technique to generate bi-directional waverforms. Theoretical error predictions for such systems using zero-crossing detectors with bandpass filtering and hysterisis (non-zero threshold) are difficult to formulate, but in progress. Empirically, this error should be much less than those produced by lack or normalization. More research on this topic is required.

Corrections for $\alpha$

As previously stated, $\alpha$ is a function of driving frequency. Figure 1.15 plots values of $\alpha$ versus heart rate for vessels ranging in radius from 1 to 5 mm. This shows the necessity for comparing heart rate as well as velocity in interpreting flow data. As an example, assume resting values are recorded for flows through an iliac artery; heart rate = 90 BPM, vessel radius = 2 mm, $\alpha = 3$. If the animal is allowed to exercise, his heart rate may reach 240 BPM. The value of $\alpha$ would then increase to five. The profile number during peak forward flow could be expected to increase from $n = 3$ to $n = 8$, under these

conditions. The mean velocity across the vessel would increase from .6 to $.8V_{max}$(during peak flow). For conditions other than whole vessel illumination, this could produce as much as a 20% change in scale factor as a direct result of changes in heart rate.

A similar analysis for flows through the renal artery produces a more encouraging result. For 20 - 25 Kg. dogs, the mean inner diameter of the renal artery is about 2.5 mm . As such, $\alpha$ will be less than 2.5 for fundamental frequencies up to 240 BPM. In addition, the artery's long length in comparison to diameter, low Renolds number, and large d.c. flow component virtually insure parabolic flow throughout the entire cardiac cycle. Continuous forward flow eliminates any possibility of directional ambiguity or normalization problems as described above. Accurate and repeatable measurement of mean cross sectional velocity can therefore be expected.

Turbulence

The transistion from laminar to turbulent flow conditions has competing effects on measurement accuracy. The velocity profile is typically blunt during turbulent flow, which by itself would reduce the zero-crossing overestimation of the net cross sectional blood velocity. Turbulence, however, also implies significant non-axial or even retrograde velocity components during peak forward flow. This produces spectral spreading and the processing errors previously described. The results from an acute calibration study with peak Renolds numbers exceeding 2500 will be reported in Section 4.

Hematocrit

Reid [13] has shown that backscattered power increases linearly with the number of scatterers. Thus increasing the hematocrit ratio from 35 to 45 volume % would only increase the audio signal to noise ratio by slightly more than 1 dB. This will be of little consequence for typical experimental conditions.

## 1.6 Area Estimation

Like the electromagnetic flowmeter [21], the Doppler flowmeter is intrinsically a velocity sensing device. A number of investigations, however, have reported linear relationships between the output of various CW systems and volume flow as determined by direct bleed-out [22,23,24]. Such calibrations are typically performed but once per animal, just prior to recovery of the transducers. Calibration by this technique is at best difficult if the animal dies unexpectedly or suffers an aortic rupture near the cuff. (Ruptures are infrequent due to the light weight of the transducer assembly).

Conversions from measured velocity to volume flow have traditionally required estimation of lumen area. Hottinger has recently described an elegant pulsed Doppler technique which obviates the need for area estimation [25]. Unfortunately, this scheme cannot be used with present commercial systems. The researcher must therefore evaluate the accuracy of his own technique for estimating lumen area. Many such methods exist including the measurement of vessel outer diameter during implantation, angiography, post-mortem pressurized silastic casts, use of one trans-

ducer element in the pulsed echo mode, or transcutaneous Doppler imaging. Diameter measurements must be made with caution, as any errors will be squared during area calculation. For example, a ± 10% accuracy in diameter measurement produces area uncertainties of approximately ± 20%. In a similar manner, a ± 30% diameter estimate produces potential area errors of ± 60% (+ 69%, - 51%). Finally, diameters should be measured in more than one plane to insure that the lumen is indeed circular.

## 1.7 Conclusions

In summary, the CW Doppler flowmeters developed during previous contract periods appear fully capable of accurate and repeatable measurements of mean cross sectional velocity for flows through the renal artery. With careful attention to transducer construction and the method of cuff attachment, errors in this measurement should be both predictable and constant. Conversions from velocity to volume flow require careful estimation of lumen area.

# IN-VITRO CALIBRATION STUDIES

2.1 A series of studies has been initiated during the past year to characterize the in-vitro performance of several Doppler systems. These studies required the development of a flow simulator with controlled acoustic and hydrodynamic properties. These properties must remain stable for weeks at a time to allow extended evaluations of flowmeter performance, and to serve as a laboratory standard for testing new flowmeter designs. Extended studies are necessary to predict the in-vivo performance and lifetime of totally implantable flowmeter systems.

The simulator has been completed but awaits testing. Consequently, long term studies or absolute flow calibrations have not been possible to date.

All of the error sources described in Section 1 of this report will need to be verified by in-vitro tests under controlled conditions.

Complex time varying spectra, as described in Section 1.5, can be generated by the apparatus shown in Figure 2.1. The Millar pressure generator is capable of producing any cyclical driving pressure at frequencies up to 200Hz. When the syringe is vented to atmosphere, oscillatory flows (described by Womersley) are possible at fundamental frequencies greater than 10Hz. Capping, or back pressurizing the syringe, allows terminations with variable compliance and reflection coefficients.

The velocity waveforms in Figure 2.2 were produced by a 2Hz square

wave forcing function, and compliant termination. This technique can also be used to check dynamic response of EMF or hot-film flowmeters.

## Acoustical Properties of Canine Aorta

3.1 The acoustical properties of canine descending aorta have been measured by in-vitro experiments. The results of the experiment allow estimations of (1) beam dispersion (Section 1.4) during passage through the vessel wall and (2) the amount of ultrasonic power required for reliable in-vivo flowmeter performance. The in-vitro data on round-trip attenuation have been verified during the acute calibration studies described in Section 4.

A large square transducer (as described by Hottinger) was placed in a water bath along with a stainless steel "point reflector". The reflector was positioned in the beam pattern at a distance of 25 cm. (Figure 3.1). Returning echoes were received by a small circular element of 4 mm diameter scribed within the larger element [25]. A reference signal was first established by transmitting 2 μsec bursts of 6 MHz ultrasound with no intervening test specimens. The signal amplitude and round-trip time delay were displayed on a high speed oscilloscope. A 2 mm thickness of canine descending aorta was then inserted between the transducer and the target. The specimen had been obtained immediately post mortem and soaked in saline until use ( 2 hrs.). The fat was stripped from the adventitia. The artery was then opened and positioned by hemostats in the ultrasonic beam.

The same experiment was repeated for a 1 mm thickness of non-reinforced silastic and a 2 mm layer of aquasonic coupling gel. The

amplitude and time delay of the original reference signal were then re-measured and found to be unchanged.

Velocity Calculations

Let $t_1$ = round trip transit time of reference signal

$t_2$ = round trip transit time with specimen in place

T = round trip transit time through specimen

$$\Delta t = t_2 - t_1 \qquad 3.1$$

Then

$$\Delta t = T = \frac{2x}{C_2} \qquad 3.2$$

where x = thickness of specimen

$C_2$ = velocity of sound in specimen

Insertion of a specimen with a given thickness removes the same thickness of water from the acoustic path. All calculations can then be made with respect to the known velocity of sound in water ($C_1$) and the thickness of the specimen (x).

$$\Delta t = 2x\left(\frac{1}{C_2} - \frac{1}{C_1}\right)$$

which becomes

$$C_2 = \frac{2xC_1}{2x + \Delta tC_1} \qquad 3.3$$

The results of these experiments are shown in Table 3.1.

Discussion

These results appear reasonable when compared with published data for other materials [26]. For the aorta, the propagation velocity closely matches the mean value for human tissue (1540 m/sec). Assuming a linear relationship between attenuation and frequency, the one way attenuation equals 1.25 dB/cm/MHz. This closely approximates the value for muscle (along fibers) of 1.3 dB/cm/MHz [26]. This figure is nearly an order of magnitude greater than for blood, but less than the value for heart muscle.

In comparison, silastic is not a good acoustical analog for vascular tissue. The velocity of sound is nearly 40% lower while the attenuation (in dB) is increased more than three-fold.

The properties of Aquasonic were studied due to its popularity as a coupling material for acute studies. Any differences from the acoustic properties of water were undetectable by our techniques. This is not surprising, however, because Aquasonic is a water based gel. As shown in Section 1.4, the angle between the incident ultrasound and the direction of blood flow will be shifted by $2^{o}$ (for $\theta = 60^{o}$) if Aquasonic is used for coupling. If this diffraction is ignored, flow velocity will then be overestimated by 6%.

Table 3.1

Acoustical Properties of Test Materials

| Material | Thickness (mm) | Δt μsec | Velocity of Sound x $10^3$ m/sec | Round-trip attenuation @ 6MHz (dB) | Round-trip attenuation per mm @ 6MHz (db) |
|---|---|---|---|---|---|
| Stripped Aorta | 2 | -.1 | 1.537 | 3 | 1.5 |
| Non-Reinforced Silastic | 1 | .7 | .975 | 5 | 5 |
| Aquasonic Coupling Gel | 2 | ^0 | 1.48 | Same as Water | Same as Water |

All measurements were made at approximately 25°C.

# IN-VIVO CALIBRATION STUDIES

## 4.1 Acute Cal Study - Series I

Two acute calibration series have been initiated during the past year. In Series I, polystrene Doppler cuffs and EMF probes were placed in series along the descending aorta of six dogs. Vessel wall thickness was assumed to be 15% of the outer diameter. After waveform comparisons, the transducers were calibrated by direct bleed-out. For 5 of the 6 animals, ±10% linearity was observed for a wide range of flow rates. Even though the cuffs were placed on vessels of similar diameters, however, the slope of the calibration curves varied by as much as 50% from one animal to the next. The study protocol proposed to identify the sources of variation follows in Section 4.2.

## 4.2 Acute Cal Study - Series II

I. Purpose: To compare and calibrate three doppler flowmeters and identify their experimental errors during acute experiments.

II. Instrumentation: EMF Flowmeter
L & M CW Doppler
Stanford CW Doppler
Stanford Pulsed Doppler
Millar Pressure Catheter

III. Parameters to track:

A. Vessel Diameter

B. Flow Profile

C. Signal to noise ratio

D. Acoustic loss through vessel walls and coupling media

E. Hematocrit

IV. Protocol (See Flow Chart - Figure 4.1)

A. The basic model is an acute preparation of an anesthetized dog with an exposed artery in the chest or abdomen.

B. The same set of transducers will be used for all animals.

C. Pulsatile waveforms will be compared between the EMF and doppler flowmeters at three different flow rates produced by graded occlusions distal to the transducers.

D. Vessel diameters will be estimated by an arteriogram for three different cases: (1) Closed Chest (2) Open Chest with Probes Attached, and (3) Open Chest After Cannulation. In addition, a pressurized silastic cast of the artery will be made at the conclusion of the experiment.

E. In vivo calibrations will be obtained by heparinization of the animal, followed by cannulation and timed collection of flow at three different flow rates. The collection period will be 10 seconds, run in duplicate at each level of constriction, with the blood returned to the animal after each run.

F. Reference Transducers: In general, a cannulating doppler probe, and the EMF flowmeter will be used as reference transducers and left undisturbed (including electrical connections) until completion of in-vivo calibrations.

G. Universal Doppler Transducer: A pair of Stanford transducers with interchangeable cuffs will be used for all doppler aortic flow measurements and calibrations. A

matched pair of transducers will be placed directly in the blood stream through the walls of the cannula. This will allow measurements of the acoustic loss through the vessel walls and coupling media. This will also help to identify beam diffraction, transducer canting, or other problems associated with the transducer-vessel interface.

H. Probe Sequence: At least two (preferably four) experiments will be run with the EMF cuff proximal to the Doppler. Thereafter, the order will be reversed for the same number of animals. All doppler transducers will point towards the heart.

I. The cannulating transducer will be driven on alternate days by the L & M and Stanford CW Systems for the duration of the flow collection procedure.

J. Flow profiles will be measured for three cases: (1) Pulsatile Arterial Flow (2) Arterial Flow After Cannulation, and (3) Flow Through the Cannula.

K. All flow data will be summarized by an on-line computer (monitor program) to allow quick checks for calibration linearity.

Results

The results for the first two studies in this Series support the theoretical predictions of Section 1. Figure 4.2 shows the mean velocity profile across a 10 mm (inner diameter) vessel at a heart rate of 120 BPM. The value of Womersley's $\alpha$ was calculated to be 9. This predicts a profile number of 10 during peak flow which closely matches the observed profile. For a fixed transducer size (3 mm) Figure 1.14 predicts a 20% overestimation of the mean cross sectional velocity. Figure 4.3 compares the observed calibration factor with this theoretical prediction. For the second animal, the measured inner diameter was 8 mm. Womersley's $\alpha$ was calculated to be 7.5, predicting a profile number of 9 during peak flow. As shown in Figure 4.4, the observed profiles closely match this prediction.

Returning again to Figure 1.14, a 22% overestimation of mean velocity was expected. As shown in Figure 4.3, the results again match the theoretical prediction.

In both studies, the round-trip acoustical loss through the vessel was measured to be 3 dB. Pulsed Doppler estimates of inner diameter matched the outer diameters of the silastic casts to within .1 mm. This study will continue, but the initial results appear to support the theoretical predictions. .

The reader is reminded that the zero-crossing detectors used in this experiment are least susceptable to statistical errors for narrow input spectra. The presence of blunt velocity profiles, and the results of real time spectral analysis (Section 5) indicate that $\alpha$ statistical errors can be expected with this set of experimental conditions. This study should be repeated, therefore, on smaller caliber vessels where lower values of $\alpha$ and broader spectra are predicted.

# REAL TIME SPECTRAL ANALYSIS

5.1 The validation of zero-crossing or first moment estimates of the mean velocity within a given sample volume, requires knowledge of the spectral distribution of the input signal. This has been demonstrated in Section 1.2.

For steady flow situations, the Doppler audio signal can be analyzed by a conventional spectrum analyzer such as an HP 8556A. The swept filter technique involves a trade-off between time resolution and frequency resolution. Adequate frequency resolution requires slow sweep speeds. For example, assume the Doppler signal bandwidth is 10 KHz and 1% resolution (i.e., 100 HZ) is required. For this typical case, one complete sweep from 0 to 10 KHz requires a full second. This is clearly unacceptable for the analysis of pulsatile flow data which may change at rates in excess of 50 Hz.

Alternatives such as fast Fourier transforms, or time compression analysis have been considered for processing the Doppler spectra. Of the two, time compression techniques offer the greatest hope for real time spectral analysis (RTSA). In addition, the requisite equipment for RTSA and computer analysis of the spectral outputs exists in-house at Ames Research Center, Moffett Field, California [27].

The time compression approach is similar to the swept filter technique, except that the signal is accepted in real time and then replayed at a much accelerated rate through a single swept filter.

The time duration of the data window is determined by the reciprocal of the resolution (i.e., bandwidth of the swept filter) required. The signals are digitized and stored in partially overlapping memories with contiguous starting times. (Figure 5.1). The contents of each memory are only analyzed for energy within a certain portion of the overall signal bandwidth. The center frequency of the swept filter is incremented between analyses until the desired frequency range has been traversed. When the time to perform a complete spectrum analysis is less than or equal to the data collection time, real time operation is achieved. These analyses are automatically performed within a Honeywell-Saicor real time spectrum analyzer.

The spectral output signals can be displayed in a variety of formats. Figure 5.2 shows one display option. A syncronization signal from the analyzer triggers a tracing on a Honeywell fiber optic recorder for each spectral analysis performed. Frequency starts on the left hand margin and increases to the right. Spectral density within the given bandwidth is indicated by z-axis modulation. This figure shows real time spectra (1 horizontal sweep each 10 msec) for Doppler flow signals for four successive heart beats. Time increases towards the top of the page. The recorder tracings have been darkened by hand to enhance reproduction.

Figure 5.3 shows comparisons between (a) the signals produced by adjacent EMF and Doppler transducers on a canine descending aorta, and (2) the spectral content of the audio input to the zero-crossing detector. For an indicated Doppler shift of 4KHz (peak zero crosser

output), the particles in the sample volume produce Doppler shifts which are evenly distributed between 2 and 6 KHz. King, Light, and Gosling have also demonstrated the value of such sonograms for transcutaneous Doppler diagnosis.

Figure 5.4 shows an alternate display format. As in Figure 5.2, frequency increases from left to right. In this case, spectral density (i.e., the relative number of scatterers) is indicated by vertical deflection. Tracings 1 - 10 show the time varying spectra for iliac Doppler signals during early systole. Figure 5.5 shows spectral changes as velocity decreases from peak flow to zero.

The centroid or mean frequency of each spectral plot can be computed by hand and compared with the corresponding flowmeter output. The preferred technique, however, is to have a computer perform these calculations off line and report comparisons between the mean frequency within the sample volume and the instantaneous flowmeter output. Such programs will be developed during the coming year and be used to evaluate the performance of present and future signal processing schemes.

# CHRONIC ANIMAL STUDIES

## 6.1 Introduction

The in-vivo performance of eleven totally implanted CW flowmeters has been thoroughly evaluated during the past contract year. This constitutes the final test for a number of design philosophies developed during previous contract periods. Several existing or potential weaknesses have been identified and eliminated. The remaining concepts have been incorporated into the design of a rugged, user oriented, totally implantable, directional flowmeter. This integrated circuit, CW design,promises significant improvements in both signal quality and user convenience. Initial prototypes will be available for use at Ames Research Center within the near future.

## 6.2 Discrete Non-Directional Systems

Eight totally implantable, non-directional flowmeters were implanted and used in physiological studies. Renal, iliac, and mesenteric blood flow velocities were measured during rest, exercise and lower body negative pressure. Typical tracings during rest, exercise and recovery are shown in Figure 6.1. The instantaneous renal velocity signal was fed to a cardiotachometer, for heart rate derivations. Within ten seconds after onset of exercise, velocities and heart rate were stabilized at new baselines. Mean renal velocities decreased 15%, mean iliac velocities increased more than 3 fold, heart rate increased

by slightly more than a factor of two. After 90 secs. of exercise, treadmill speed was increased and held constant until the end of the five minute exercise study. These results are not unexpected. They do, however, demonstrate the ability to telemeter clean, uninterrupted flow signals from multiple units implanted in an exercising animal.

# EVALUATION OF AN INTEGRATED CIRCUIT, TOTALLY IMPLANTABLE, BIDIRECTIONAL CW DOPPLER FLOWMETER

The in-vivo performance of a totally implanted, integrated circuit, bidirectional CW Doppler flowmeter has been tested at Ames Research Center during the last year [12]. Three flowmeters were implanted with the Doppler probe immediately adjacent to a Zapeda EMF flow transducer. The EMF leads were externalized at the base of the neck to allow beat by beat waveform comparisons.

The tracings in Figure 7.1 show the results of such a study one month after implantation. This unit functioned reliably until failure of the transducer cable, two months after implantation.

As previously stated, many of the design concepts proven in this test have been included in an upgraded version of a similar system.

The chronic problem of transducer cable breakage has been eliminated by use of a commercially available, stainless steel coaxial cable. This will greatly increase the implanted lifetimes for present and future implantable Doppler systems.

# DOPPLER MITRAL FLOW TRANSDUCER

A new Doppler mitral flow transducer has been developed for measuring flow across the mitral valve in chronic animal preparations. The transducer is constructed from a stainless steel ring, a cast epoxy pedestal, and LTZ-2 piezoelectric material (Figure 8.1). The transducer elements are coated with a $\frac{1}{4}$ wave matching layer and backed with a layer of echospheres for efficient operation in the pulsed mode. The transducers are molded onto the pedestal, which is epoxed to the stainless steel ring. The ring is then covered with dacron mesh and sewn into the mitral annulus above the mitral valve (Figure 8.2).

This transducer has been calibrated for measurement of mitral flow at rest and during lower body negative pressure. The results of the study have been published during the past contract year [28]. The transducer allows chronic measurements of previously unavailable mitral flow parameters: Pulsed Doppler operation allows real time display of the time varying velocity profile (above the valve) throughout the cardiac cycle (Figure 8.3). The orthogonal placement of transducers around the ring allows these measurements both along and across the valve commissures (Figure 8.4). Sequential use of the three transducers allows triangulation to determine the orientation of the center flow velocity vector with respect to the mitral annulus. Changes in this vector can then be computed throughout the cardiac cycle for a variety of physiologic states. The echo information inherent in the pulsed

Doppler video signal can be displayed and recorded by fiber optic recorders to provide a real time, hard copy record of relative motion between the transducers and the opposing atrial structures. Multiplexing of the range gate markers onto this display would document the diameter across which flow was measured.

The tracings in Figure 8.5 show the amplitude and timing of typical center velocity waveforms recorded by the CW technique. Both passive and active ventricular filling can be seen. The waveforms show close agreement with published EMF waveforms [29], and mitral echocardiograms [30].

Figure 8.6 shows typical mean velocity profiles recorded along the axis of the commissures. A-scan echo information is recorded in the top tracing while the gate location and mean velocity at that location appear beneath.

Figure 8.7 shows simultaneous tracings from 6 locations across the commissures of another animal. These signals were produced by a totally implantable, non-directional pulsed Doppler flowmeter [3]. In this case, the flow profile is observed to be nearly blunt throughout the entire cardiac cycle.

In summary, the transducers can be operated in either the CW (Figure 8.8) or pulsed mode, with external or totally implanted electronics to provide new information on the hemodynamics of flow through normal and prosthetic valves in the chronically instrumented animal. Modifications of ring construction would allow its use to measure venous return through the tricusped valve during centrifugation, exercise or lower body

negative pressure. The anticipated advances in signal display techniques will be directly applicable to conventional pulsed Doppler systems.

# DATA COLLECTION TECHNIQUES

Researchers from Stanford and NASA have also collaborated to evaluate techniques for the automatic collection and analysis of telemetered physiological data. This work is a necessary prelude for many extended research protocols where direct interactions between experimentor and subject are either undesireable (circadian rhythm studies) or impossible (as in space flight). The results of that research are summarized in the Appendix.

## REFERENCES


[1] Annual Report, NASA Grant NGR-05-020-615, September 1973

[2] Semi-Annual Report, NASA Grant NGR-05-020-615, July 1974

[3] Robert W. Gill, "An Implantable Pulsed Doppler Ultrasonic Flowmeter Using Custom Integrated Circuits", Ph.D. Thesis, Stanford University, May 1975.

[4] W. R. Brody and J. D. Meindl, "Theoretical Analysis of the CW Doppler Ultrasonic Flowmeter", IEEE Trans. on Biomedical Engineering, Vol. BME-21, No. 3, May 1974. pp. 183-192.

[5] R. S. Reneman and M. P. Spencer, "Difficulties in Processing an Analog Doppler Flow Signal; With Special Reference to Zero-Crossing Meters and Quantification", Cardiovascular Applications of Ultrasound, R. S. Reneman, Editor, 1974, pp. 32-42.

[6] R. D. Bauer, T. Pasch, W. Sperling, "Studies on the Accuracy of Directional Doppler Flowmeters with Regard to Steady and Pulsatile Flow", Proc. of the Second World Congress on Ultrasonics in Medicine, Excerpta Medica, Amsterdam, 1974, pp. 290-294.

[7] S. W. Flax, J. G. Webster, S. J. Updike, "Pitfalls Using Doppler Ultrasound to Transduce Blood Flow", IEEE Transactions on Biomedical Engineering, Vol. BME-20, No. 4, July, 1973. pp. 306-309.

[8] S. O. Rice, "Mathematical Analysis of Random Noise", Bell System Technical Journal, #23 1944, 282-332.

[9] S. G. Flax, J. G. Webster, S. J. Updike, "Statistical Evaluation of the Doppler Ultrasonic Blood Flowmeter", I.S.A. Transactions, Vol. 10 No. 1. pp. 1-20.

[10] W. R. Brody, "Theoretical Analysis of the Ultrasonic Blood Flowmeter", SEL Report # 71-049, Ph.D. Thesis, 1971, Stanford University.

[11] D. M. DiPietro, "Monolithic Integrated Circuits for an Implantable Continuous Wave Ultrasonic Blood Flowmeter", SEL Technical Report # 4958-2, Ph.D. Thesis, 1974, Stanford University.

[12] Bert L. Frescura, "Integrated Circuits for an Implantable Bidirectional Ultrasonic Flowmeter", Ph.D. Thesis, Stanford University, May 1975.

[13] J. M. Reid, R. A. Sigelmann, M. G. Nasser, D. W. Baker, "The Scattering of Ultrasound by Human Blood", Proc. Eigth ICMBE, 1969.

[14] S. G. Flax, Webster, Updike, "Noise and Functional Limitations of the Doppler Blood Flowmeter", Cardiovascular Applications of Ultrasound. R. S. Reneman, Editor. American Elsevier Publishing Co. New York, 1974 pp. 18-31.

[15] E. O. Attinger, Pulsatile Blood Flow , McGraw Hill Book Company, New York, 1964.

[16] L. Gerzberg, J. D. Meindl, "Mean Doppler Shift Detector for Simultaneous Forward and Reverse Flow-Velocity Measurement", Proc. 28th ACEMB, New Orleans, Sept. 1975.

[17] Sales Literature, Directional Doppler for Vascular Surgeons, Model 806, Parks Electronics Laboratory, 12770 S. W. First, Beaverton, Oregon 97005.

[18] John R. Womersley, "An Elastic Tube Theory of Pulse Transmission and Oscillatory Flow in Mammalian Arteries", WADC Technical Report 56-614, 1957.

[19] Phillip J. Bendick, "A Laser Doppler Study of Velocity Profiles in Oscillatory Flow", Ph.D. Thesis, Stanford University, March 1973.

[20] Donald A. McDonald, "Blood Flow in Arteries", Edward Arnold Ltd., London, 1960

[21] D. H. Bergel, U. Gessner, "The Electromagnetic Flowmeter", Methods in Medical Research, Vol. 11, Year Book, Medical Publishers, Inc., Chicago, 1966, pp. 70-82.

[22] S. F. Vatner, D. Franklin, S. Van Citters, "Simultaneous Comparison and Calibration of the Doppler Ultrasonic and Electromagnetic Flowmeters", Journal of Applied Physio., Vol 29, No. 6, 1970. pp. 907-910.

[23] F. D. McCleod, Calibration of CW and Pulsed Doppler Flowmeters", Proc. 23rd. ACEMB, 1970

[24] R. F. Rushmer, D. W. Baker, H. F. Stegall, "Transcutaneous Doppler Flow Detection as a Nondestructive Technique", J. Appl. Physio., 21(2), pp. 554-556, 1966.

[25] C. F. Hottinger, J. D. Meindl, "An Ultrasonic Technique for Unambiguous Measurement of Blood Volume Flow", Proc. IEEE Ultrasonics Sympo., Milwaukee, Wisconsin, 1974.

[26] P. N. T. Wells, Physical Principles of Ultrasonic Diagnosis, Academic Press, London, 1969.

[27] H. Finger, J. Anliker, T. Rimmer, "A Real-Time Phase Vector Display for EEG Monitoring", Proc. 26th ACEMB, Minneapolis, Minn, 1973.

[28] E. Carlson, W. Freund, H. Sandler, J. Meindl, "Doppler Measurement of Mitral Flow at Rest and During Lower Body Negative Pressure", Proc. 10th Annual AAMI Meeting, Boston, 1975.

[29] S. Nolan, S. Dixon, R. Fisher, A. Morrow, "The Influence of Atrial Contraction and Mitral Valve Mechanics on Ventricular Filling," Amer. Ht. Journ. Vol. 77, No. 6, 1969, pp. 784-791.

[30] S. Laniado, E. Mellin, M. Kother, L. Levy, J. Stadler, R. Terdiman, "A Study of the Dynamic Relations Between the Mitral Valve Echogram and Phasic Mitral Flow Circulation", Vol. 51, January 1975, pp. 104-113.

## Contributing Staff

William R. Freund
Research Engineer

James D. Meindl
Principal Investigator, Director Stanford Electronics Laboratories,
Stanford University

William L. Beaver
Associate Director, Center for Integrated Electronics in Medicine,
Stanford University.

42.2

# A SYSTEM FOR THE AUTOMATIC COLLECTION AND ANALYSIS OF TELEMETERED PHYSIOLOGICAL PARAMETERS

W. R. Freund, Stanford Electronics Laboratories, Stanford, Calif.
E. P. McCutcheon*, T. B. Fryer*, H. Sandler*

A number of special experimental protocols require long term data sampling from unrestrained, free ranging animals. High data density is often required, especially for the detection and classification of aperiodic events. Obtaining physiological data for long durations at controlled sampling rates requires special system capabilities. Chronically implanted transducers or telemetry packs must be sufficiently durable to withstand the internal environment and sufficiently nonreactive to be tolerated for indefinite periods of time. Data acquisition and transmission links must be completely reliable and capable of operation with minimum attention. Automatic data analysis is mandatory to compress the weeks of data often collected. To satisfy these criteria, a monitoring system has been designed which allows automatic data collection and analysis on either a continuous or periodic basis from appropriately instrumented animals. The information can be preserved by an analog tape recorder for off-line processing on a large computer, or sent directly to a mini-computer (PDP-12) for on-line analysis and data reduction.

In a representative application to cardiovascular research, multiplexing and transmission of the various pressure, EKG and flow signals are accomplished by use of a miniature, multi-channel telemetry system (1). The parameters of interest can be continuously transmitted by a backpack system with percutaneous leads or by a totally implanted telemetry system (2). In the latter case, current drain from the implanted batteries can be minimized by transmitting only a few minutes of data each hour. In this mode, periodic switching is accomplished by a timed oscillator which transcutaneously controls the operation of the implanted unit. With an increase of power, the oscillator can also be used to recharge the implanted batteries between transmission periods.(3).

After transmission, the RF signals are amplified and routed to an FM receiver located at the terminal processor. There the PWM information is demultiplexed, combined with a time code, and routed to an on-line computer and to various recording devices. When the switching oscillator is employed, a tone detector monitors the receiver output. When the PWM subcarrier appears, the tone detector signals the beginning of a new record to the tape recorder or computer.

Several options are available for data compression and analysis. An on-line computer logs mean values and screens for selected parameters from each beat. Mean values are determined for 10-second intervals or for integral multiples of 10 seconds. These are stored, and multiple display formats are available.

Off line analysis with either the PDP-12 or larger computers can be used to screen rapidly for ectopic beats. In addition, the trend analysis indicates data blocks requiring more detailed examination. The large computer is programmed to analyze twenty or more cardiovascular variables such as pulse wave velocity, stroke work and power, and dp/dt on a beat-by-beat basis for each data block selected.

The data shown below were collected automatically with the system described:

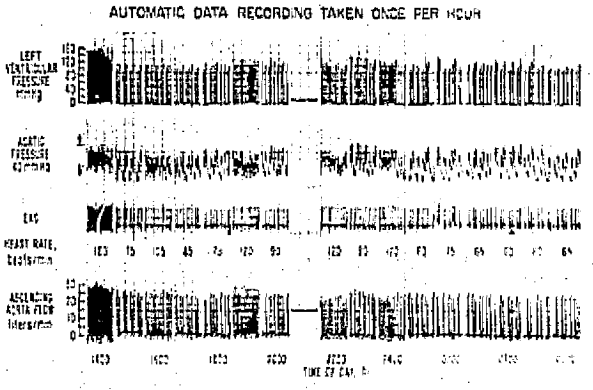


The system as described has many uses. At the present time it is providing information concerning circadian rhythms and the effects of drugs on the cardiovascular system.

REFERENCES:
1. Freund, W. R., T. B. Fryer, H. Sandler. A miniature multi-channel telemetry system for physiological monitoring. Proc, 26 ACEMB, 1973.
2. McCutcheon, E. P., E. Carlson, T. B. Fryer, H. Sandler. An implantable multi-channel telemetry system for obtaining data from free-ranging animals. Assn. Adv. Med. Inst., New Orleans, April 1974.
3. Fryer, T. B., H. Sandler, A rechargable battery system for implantable telemetry systems. Proc. 23 ACEMB, 1970.

This work was partially funded by NASA grant NGR 05-20-615 and NIH Grant NIH-GM-1790-04.

Stanford Electronics Laboratories
Stanford University
Stanford, California 94305

* NASA, Ames Research Center
Biomedical Research Division
Moffett Field, California 94035

PRECEDING PAGE BLANK NOT FILMED

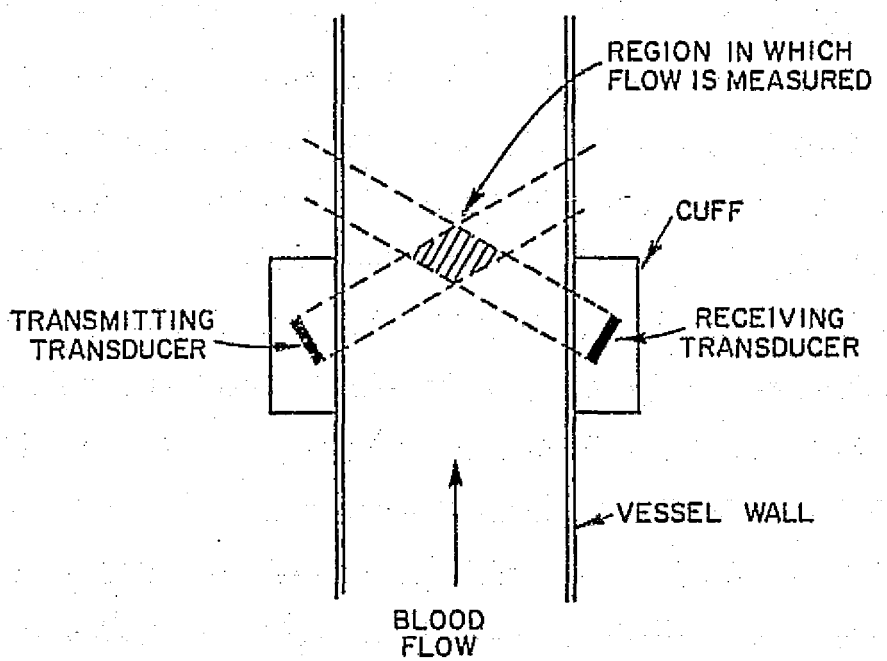


FIG 1.1 CW DOPPLER PERIVASCULAR TRANSDUCER

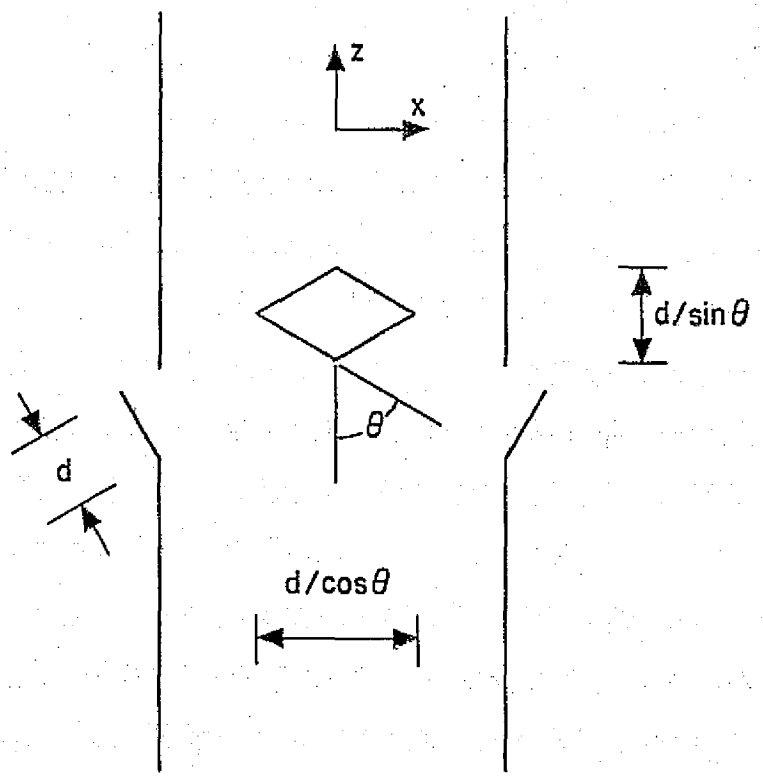


FIG 1.2 CW SAMPLE VOLUME GEOMETRY

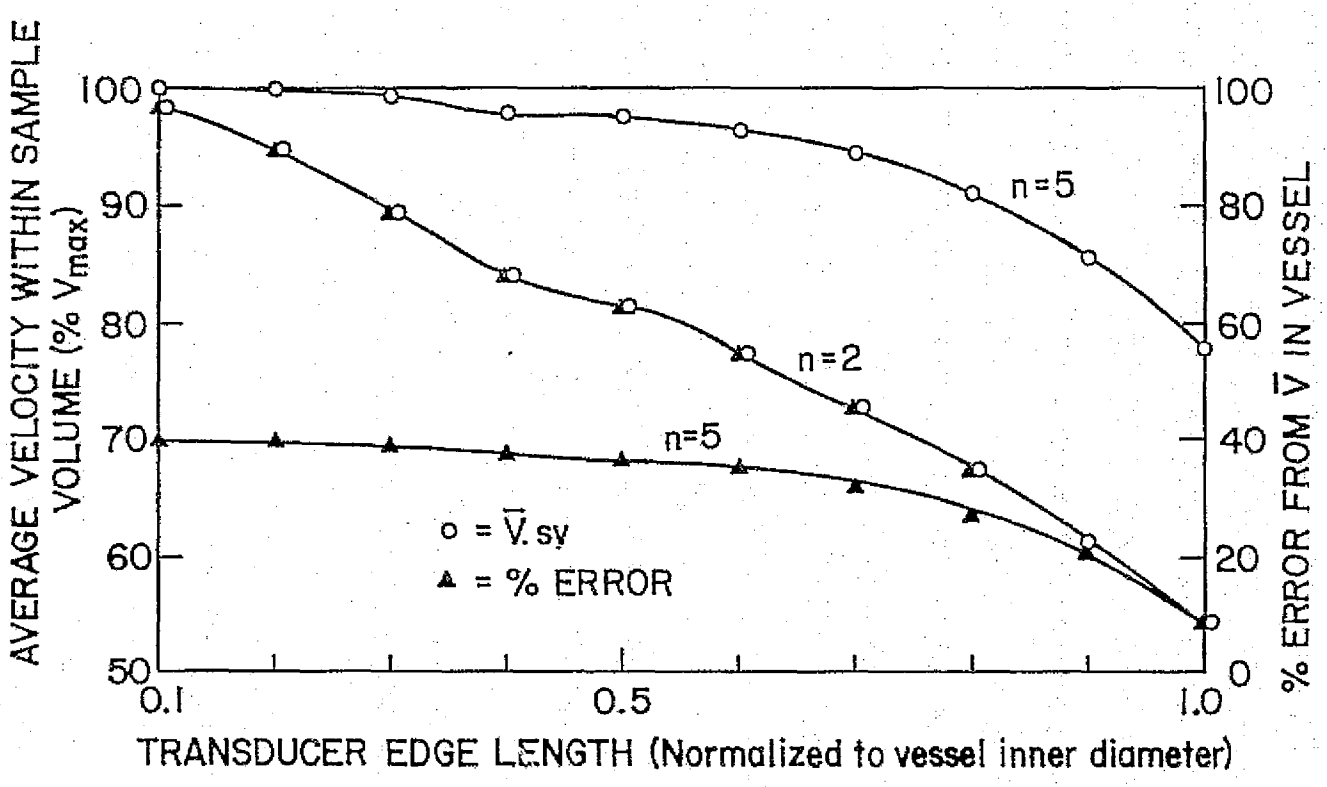


FIG 1.3 AVERAGE VELOCITY WITHIN SAMPLE VOLUME VS TRANSDUCER SIZE
SQUARE TRANSDUCERS
$\theta = 60°$

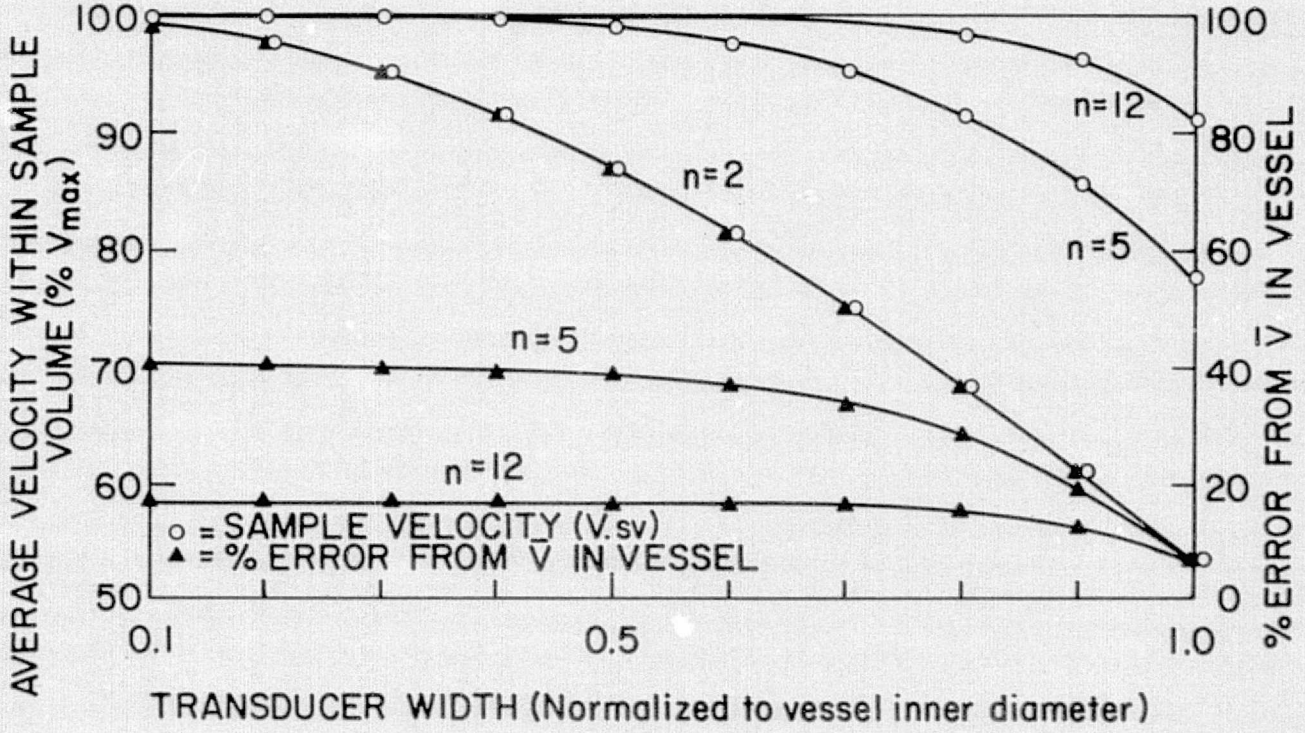


FIG 1.4 AVERAGE VELOCITY WITHIN SAMPLE VOLUME VS TRANSDUCER SIZE
RECTANGULAR TRANSDUCERS: WIDTH = (2 × HEIGHT)
$\theta = 60°$

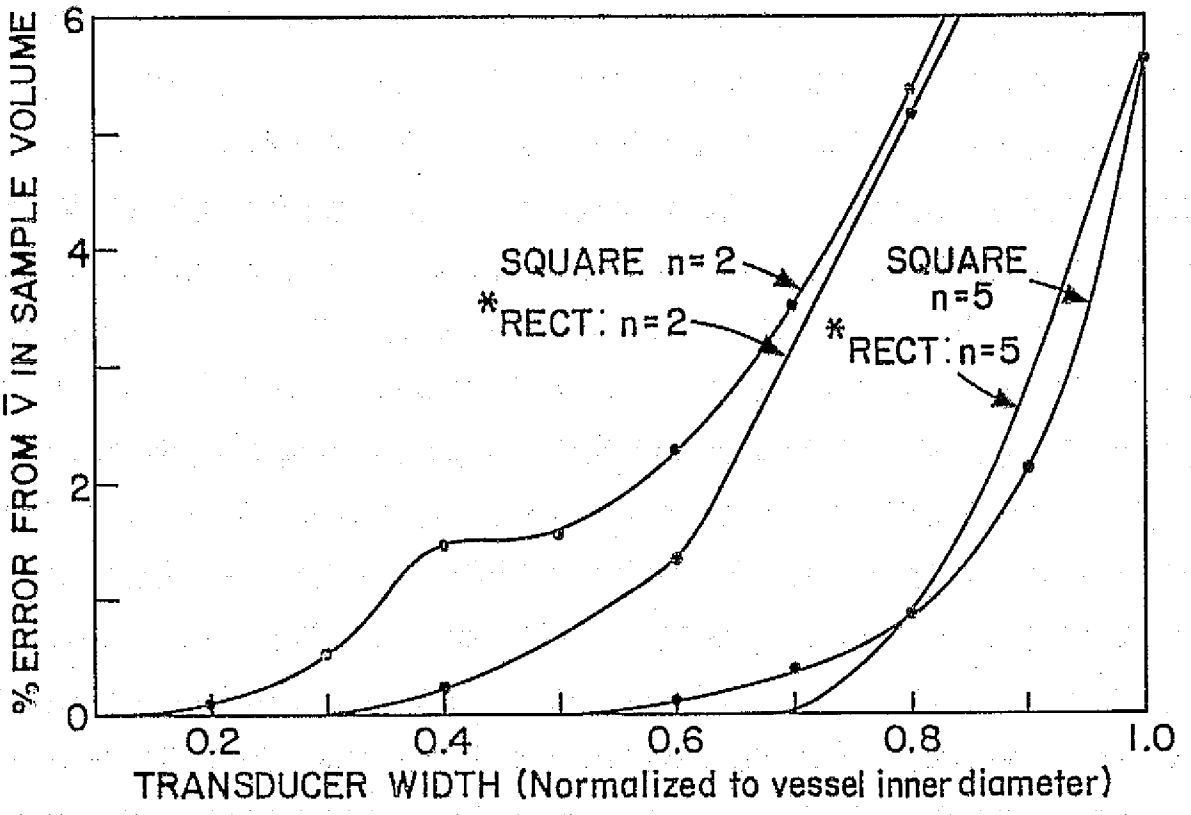


*Width = 2 × height

FIG 1.5 ZERO CROSSING OVERESTIMATION OF $\bar{V}$ WITHIN SAMPLE VOLUME VS TRANSDUCER EDGE LENGTH

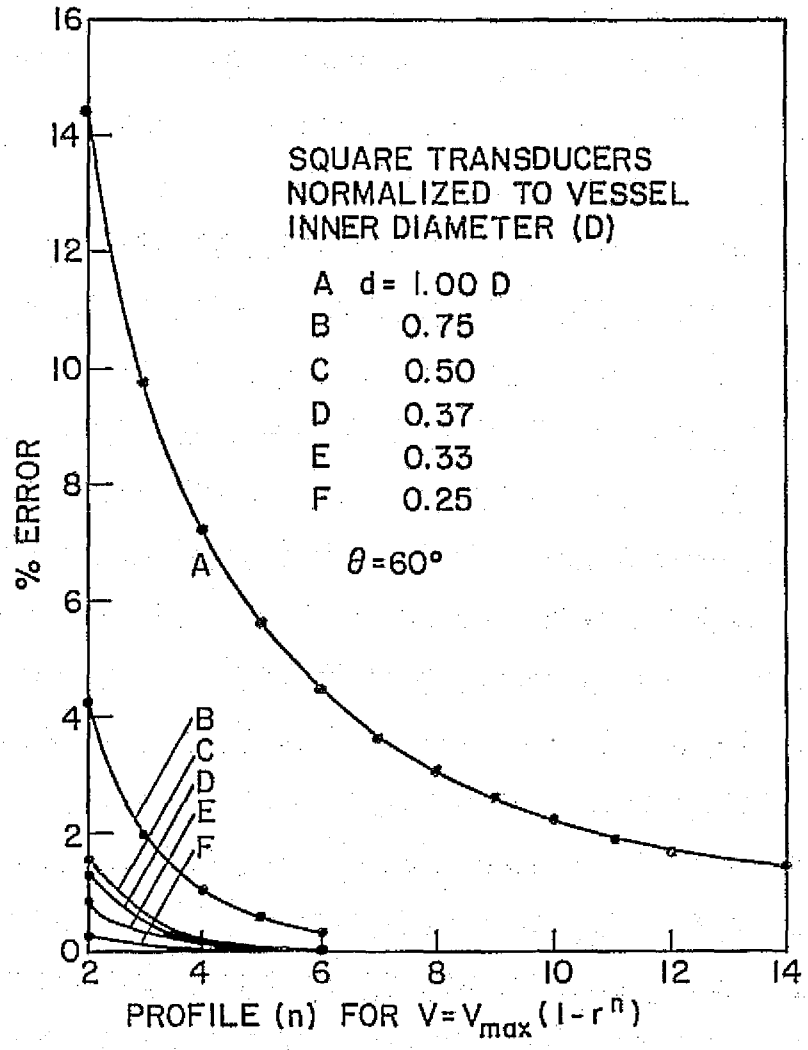


FIG 1.6 ZERO CROSSING OVERESTIMATION OF $\overline{V}$ WITHIN SAMPLE VOLUME VS PROFILE NUMBER (n) AND TRANSDUCER EDGE LENGTH (d)

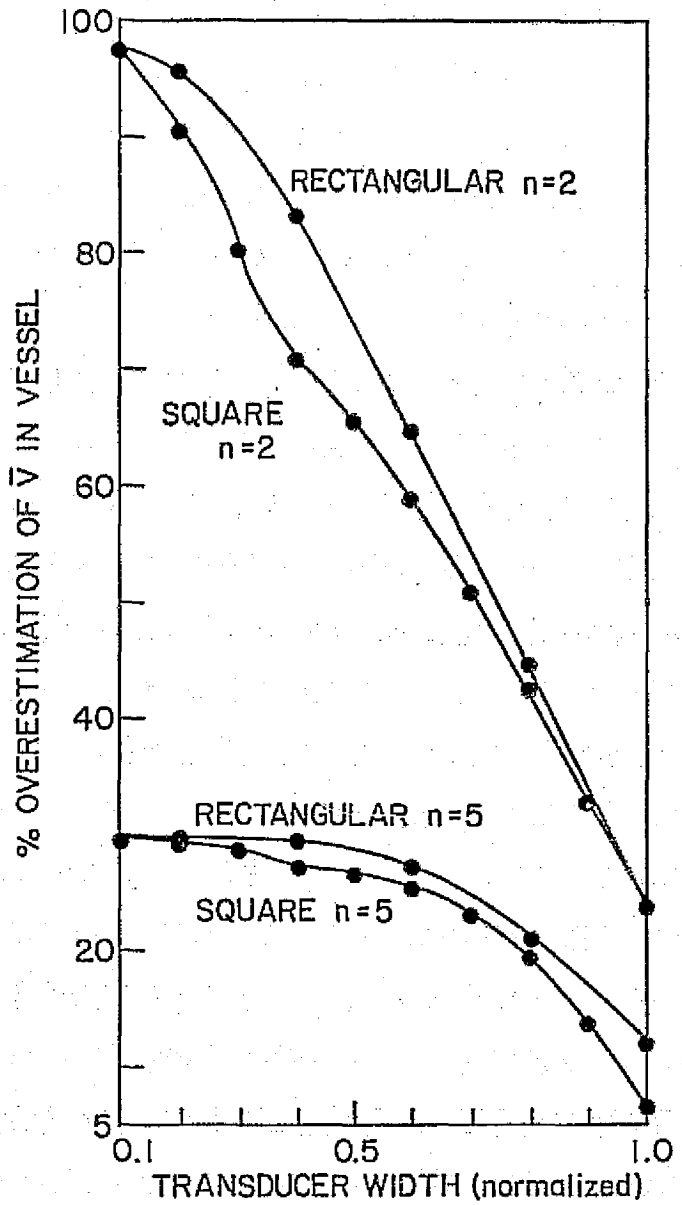


FIG 1.7 ZERO CROSSING OVERESTIMATION OF $\bar{V}$ IN VESSEL VS TRANSDUCER SIZE

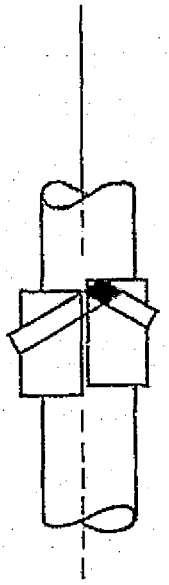

FIG 1.8 SHIFTING OF SAMPLE VOLUME DUE TO AXIAL OFFSETS

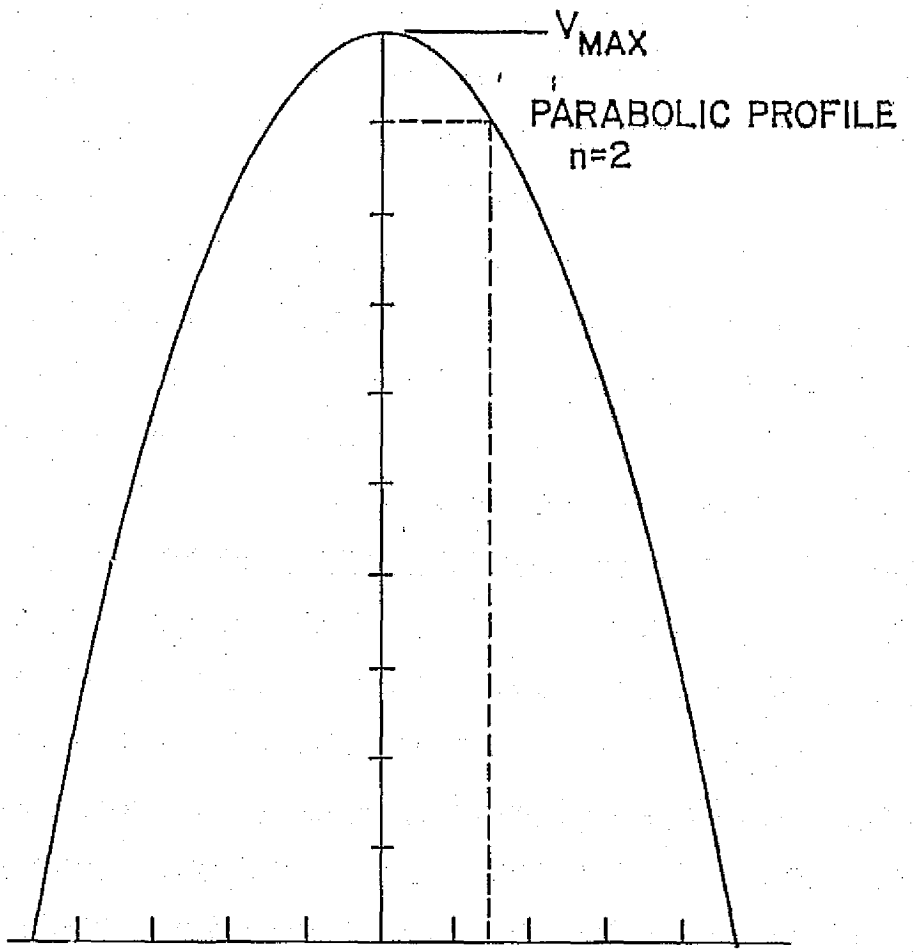


FIG 1.9a REDUCTION OF SAMPLED VELOCITY DUE TO AXIAL OR ANGULAR OFFSETS

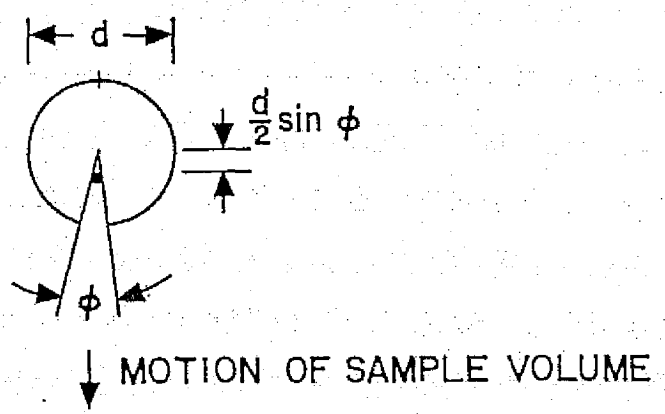


FIG 1.9b MOTION OF SAMPLE VOLUME DUE TO ANGULAR OFFSET

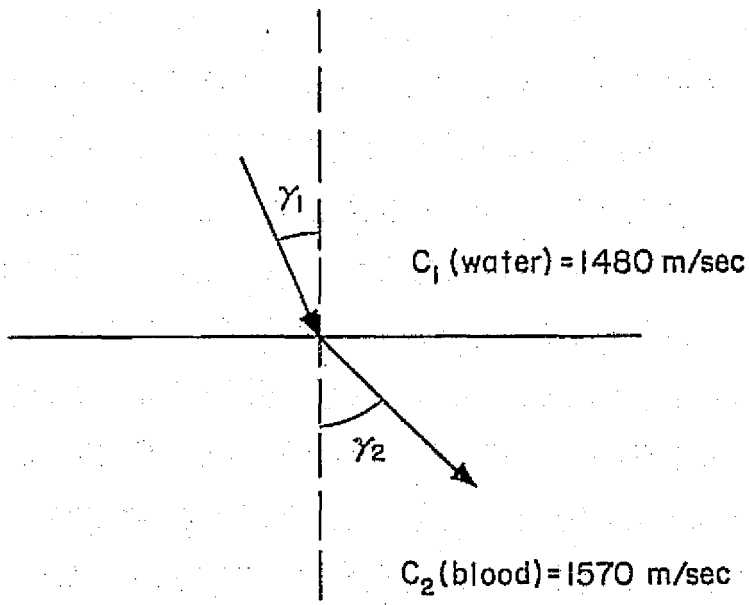


Snell's Law: $$\frac{\sin \gamma_1}{\sin \gamma_2} = \frac{C_1}{C_2}$$

FIG 1.10 ULTRASONIC BEAM REFRACTION

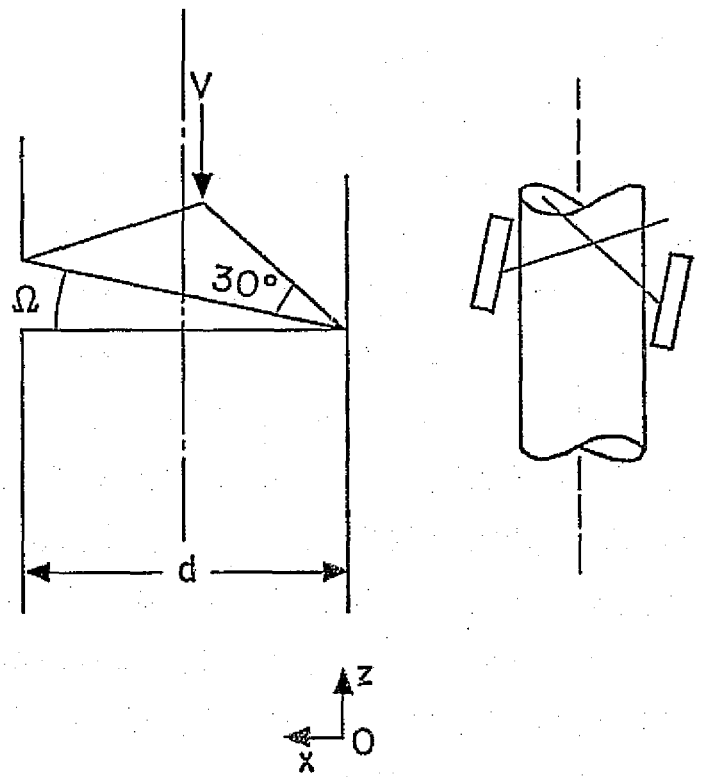


FIG 1.11a EFFECTS OF CUFF CANTING ON SAMPLE VOLUME LOCATION

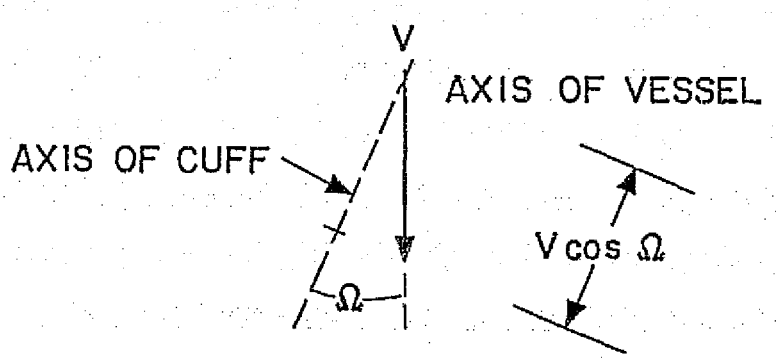


FIG 1.11b COMPUTATION OF VELOCITY COMPONENTS ALONG AXIS OF CUFF

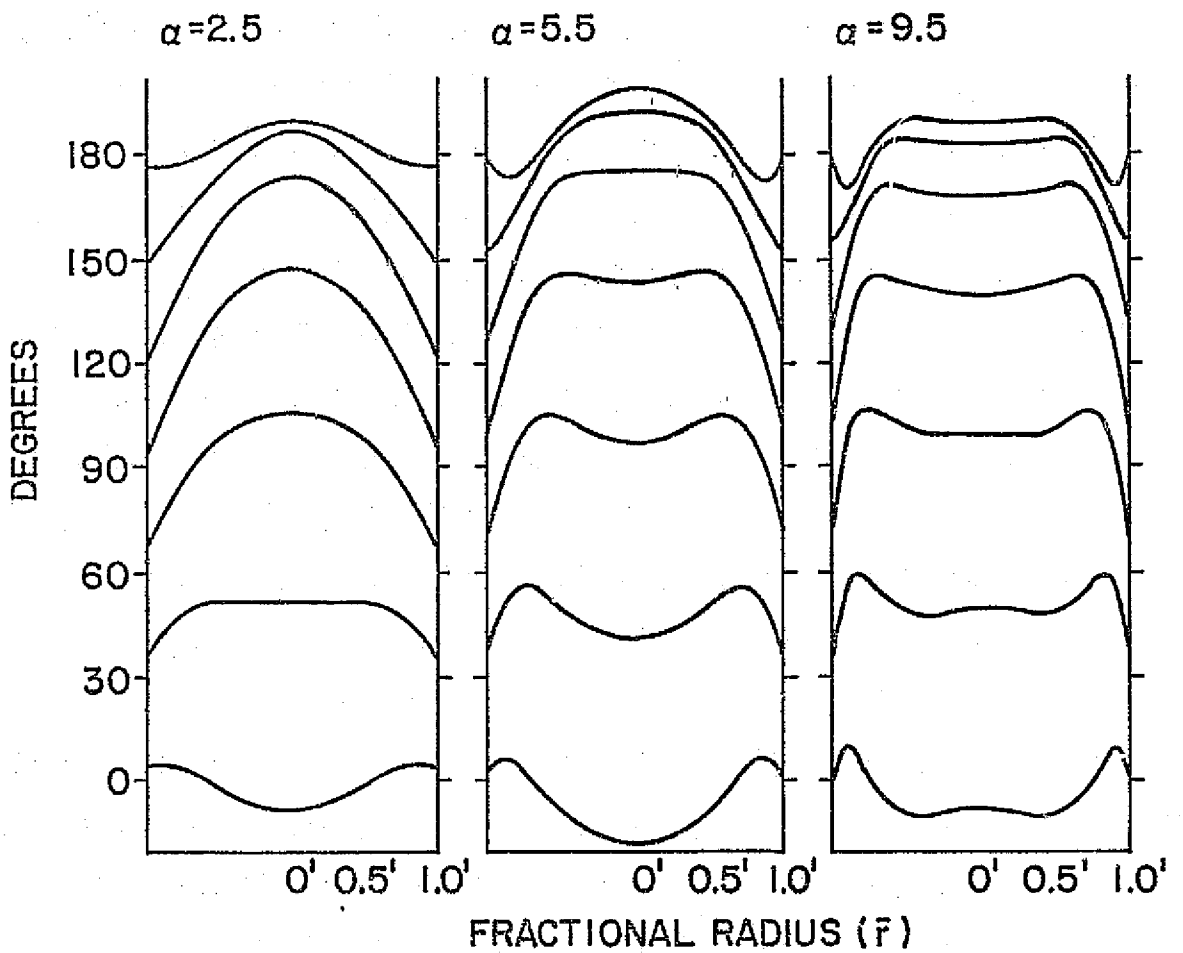


FIG 1.12 TIME VARYING VELOCITY PROFILES WITH SINUSOIDAL FORCING FUNCTIONS (From Bendick [19])

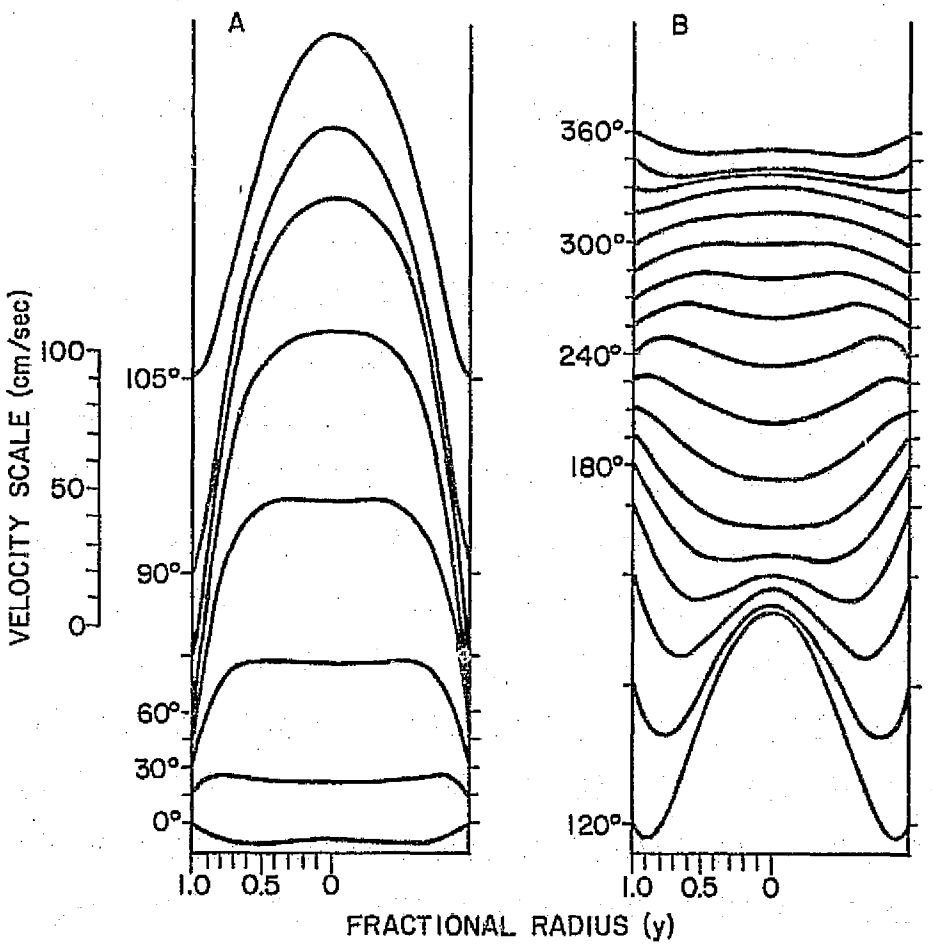


FIG 1.13 VELOCITY PROFILES CALCULATED FROM THE MEASURED PRESSURE GRADIENT IN THE FEMORAL ARTERY OF THE DOG (From MacDonald [20])

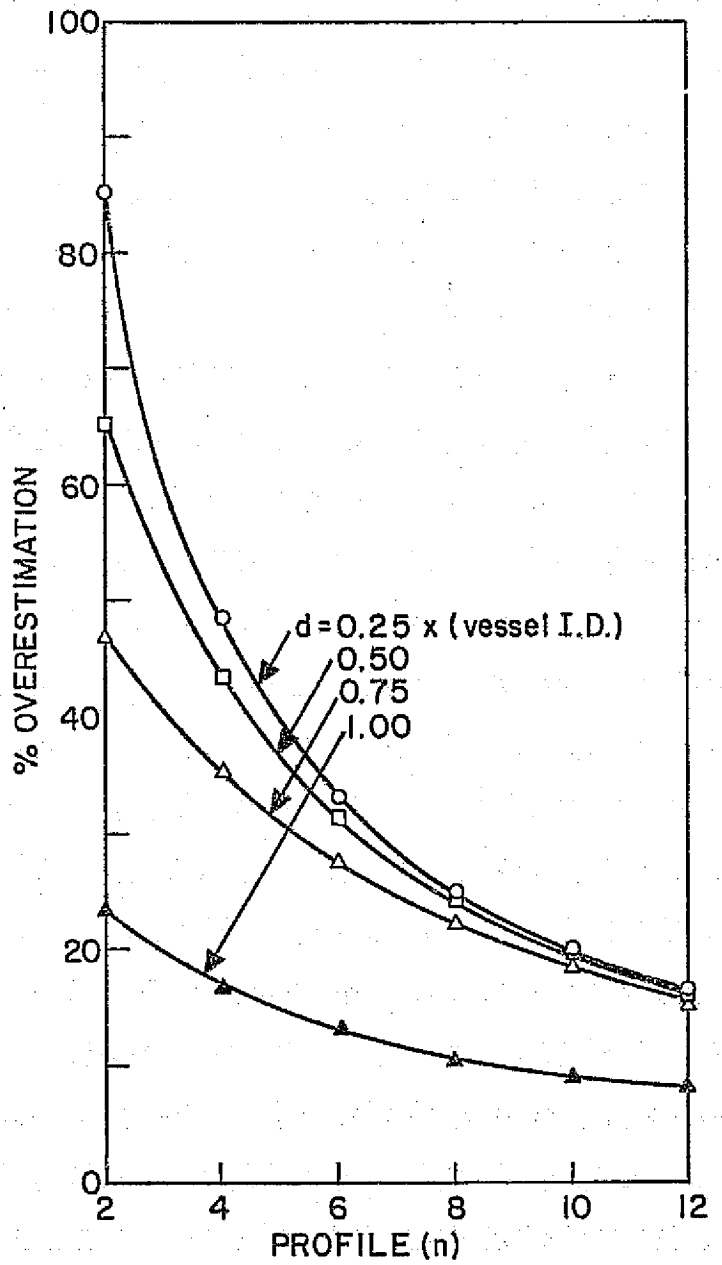


FIG 1.14 ZERO CROSSING OVERESTIMATION OF $\overline{V}$ WITHIN VESSEL VS PROFILE NUMBER (n) VS TRANSDUCER EDGE LENGTH (d)

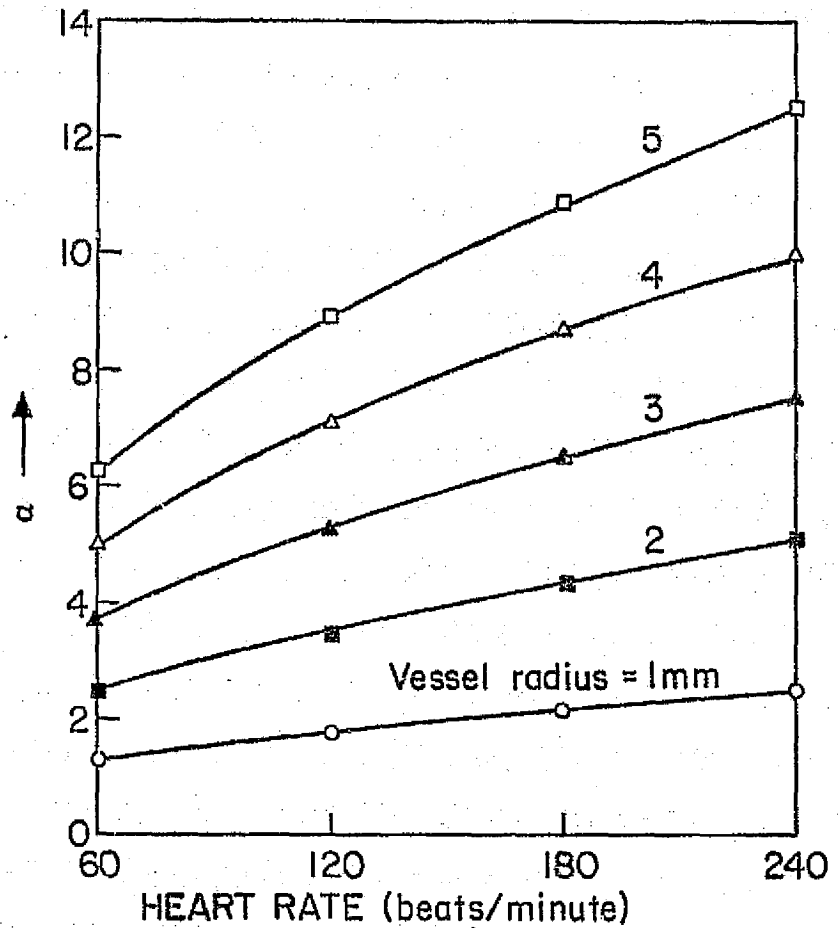


FIG 1.15 INDEX OF PULSATILITY ($\alpha$) VS FORCING FREQUENCY

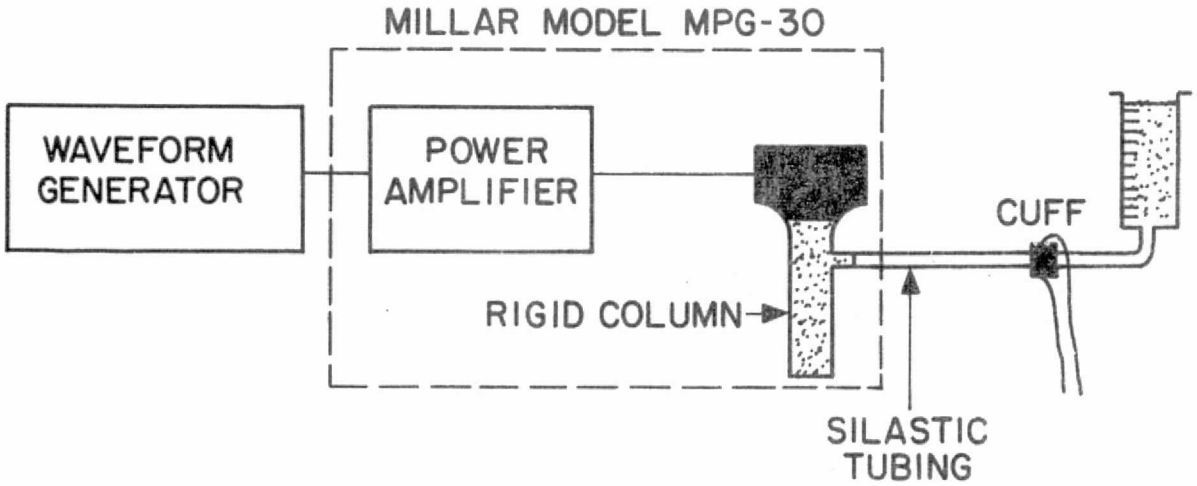


FIG 2.1 DYNAMIC FLOW SIMULATOR

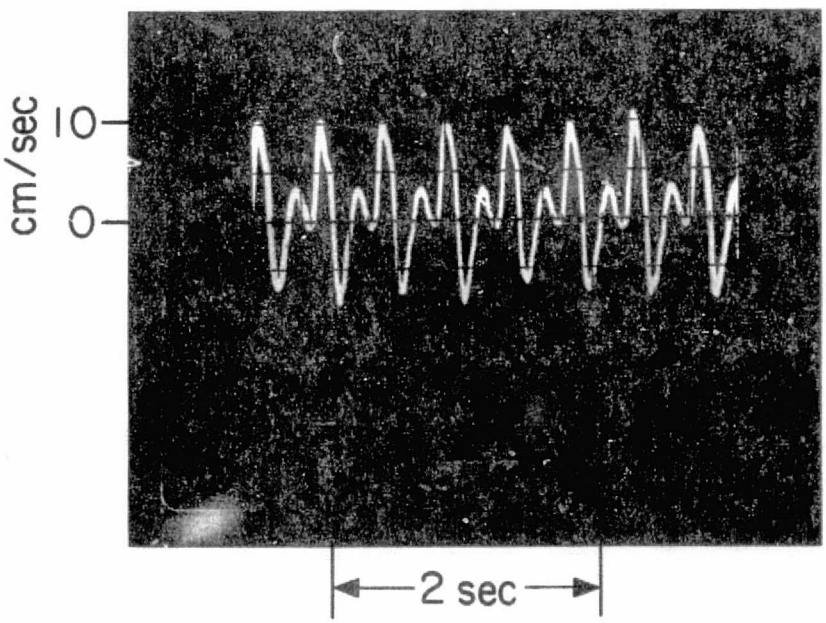


FIG 2.2 VELOCITY TRACINGS PRODUCED BY A DIRECTIONAL CW DOPPLER FLOWMETER ON THE DYNAMIC FLOW SIMULATOR

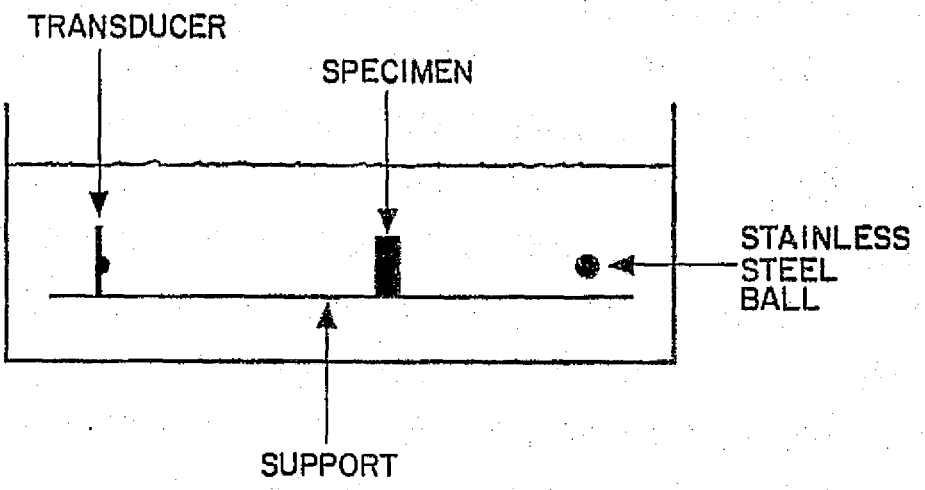


FIG 3.1 EXPERIMENTAL SET-UP FOR TESTING AORTIC ACOUSTICAL PROPERTIES

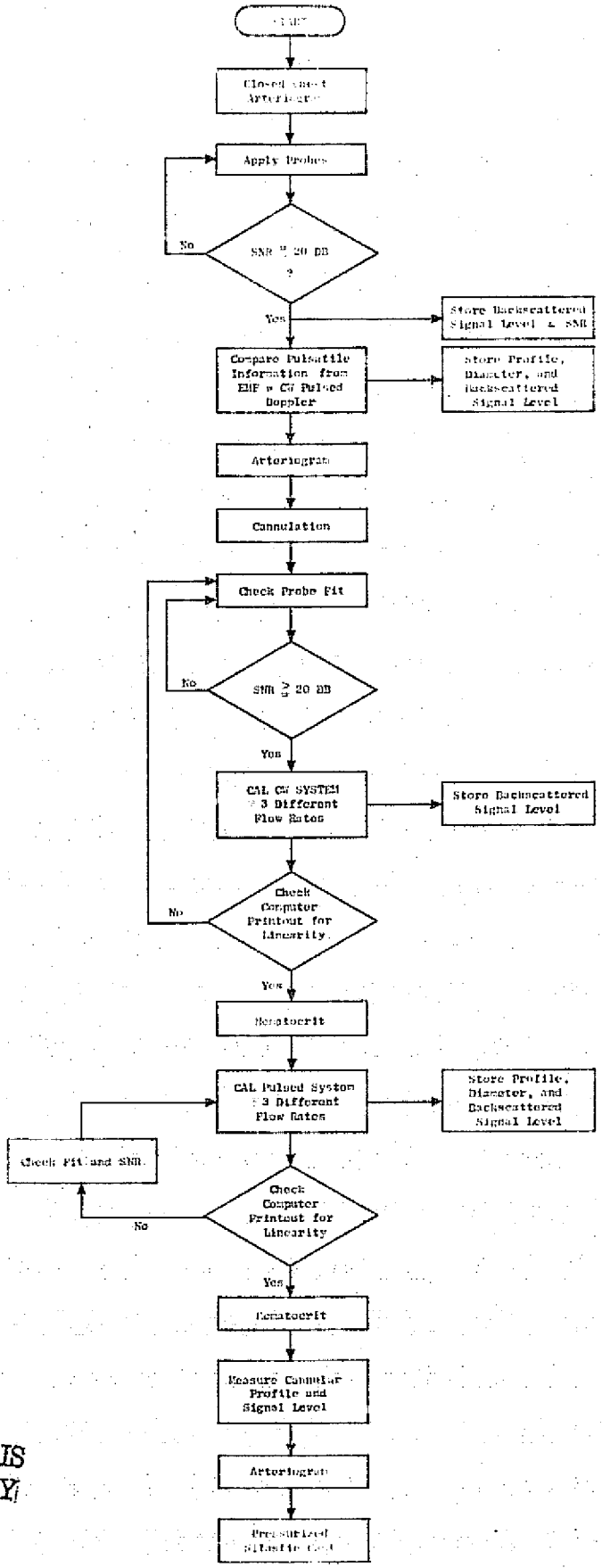




FIG 4.1 ACUTE CAL PROTOCOL-FLOW CHART

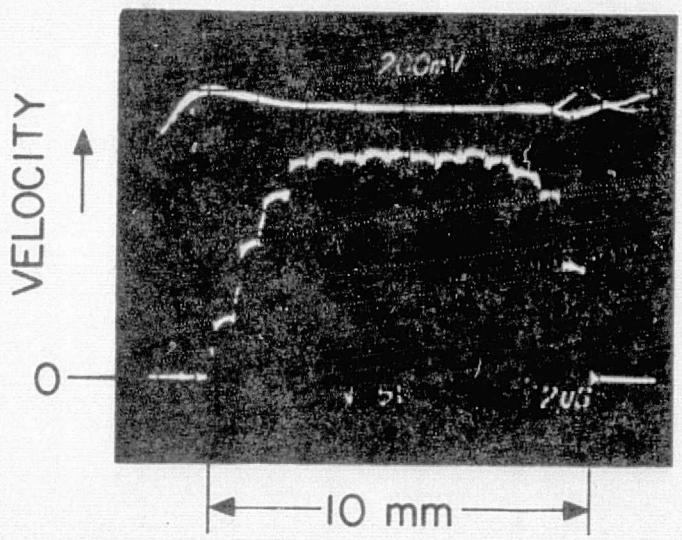


FIG 4.2 MEAN VELOCITY PROFILE--CAL SERIES II, STUDY I

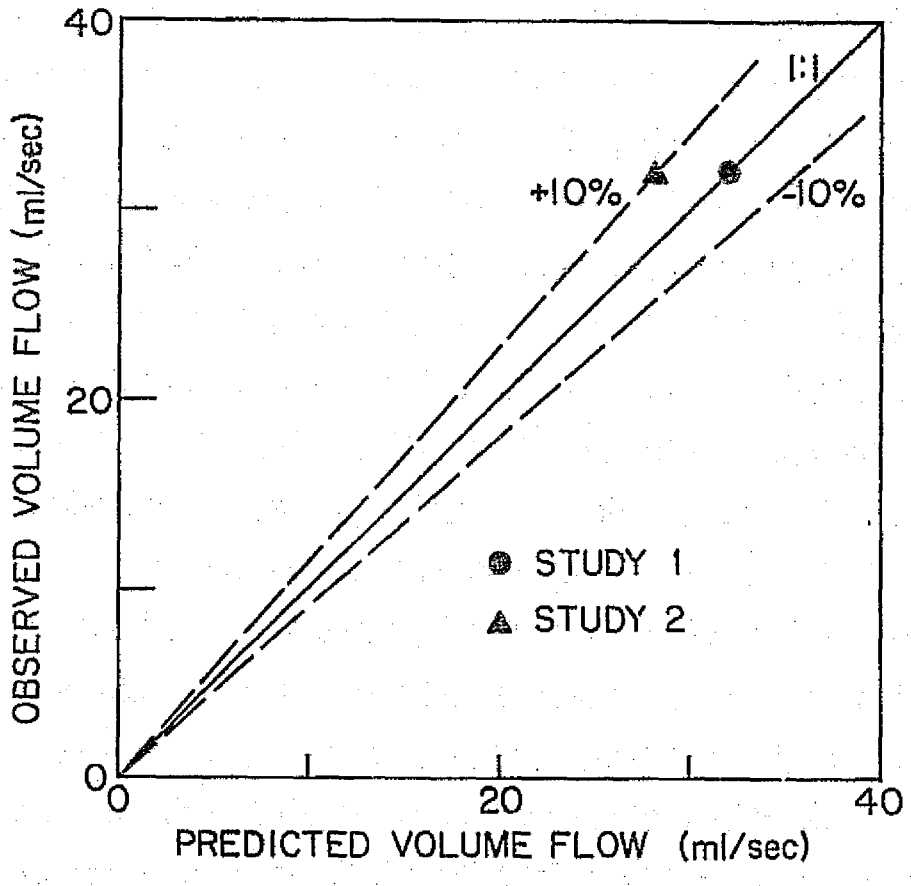


FIG 4.3 THEORETICAL VS OBSERVED CAL FACTORS FOR CW FLOWMETERS ON DESCENDING AORTA--CAL SERIES II

1 CAL = 2 KHz Doppler Shift
= 50 cm/sec

*Q = K (50 cm/sec) (Measured Cross Sectional Area) (see text for calculation of K)

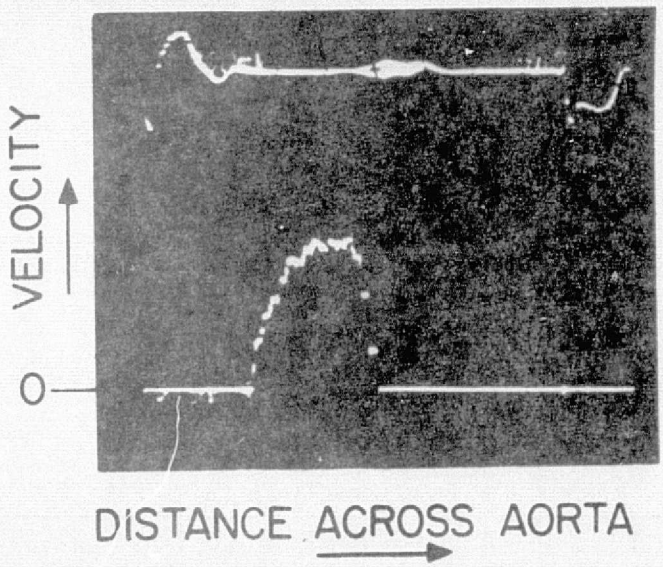


FIG 4.4 MEAN VELOCITY PROFILE--CAL SERIES II, STUDY II

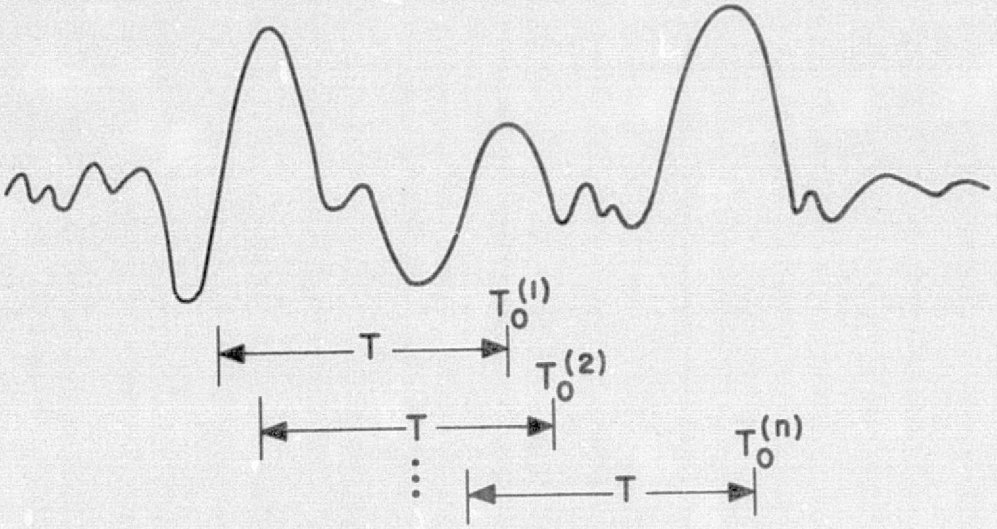


FIG 5.1 DATA INPUT FOR REAL TIME SPECTRAL ANALYSIS

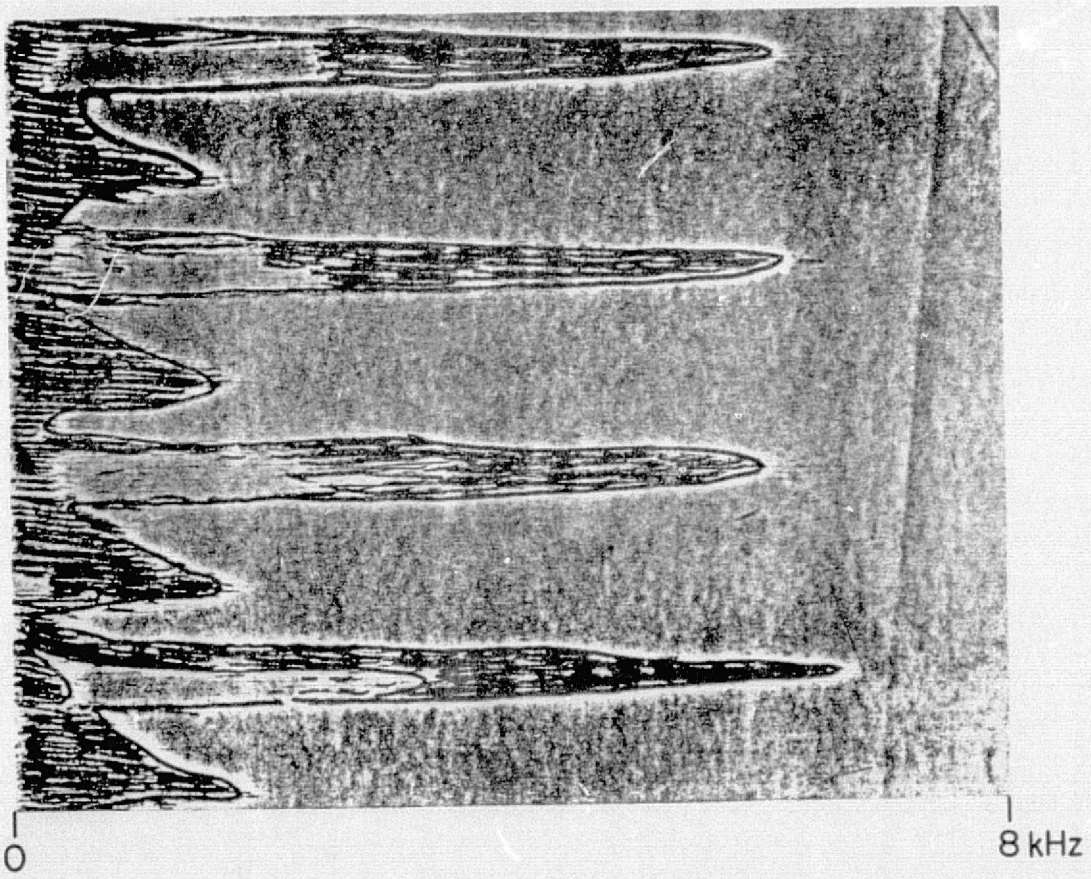


FIG 5.2 FIBER OPTIC RECORDER DISPLAY OF TIME VARYING DOPPLER SPECTRA

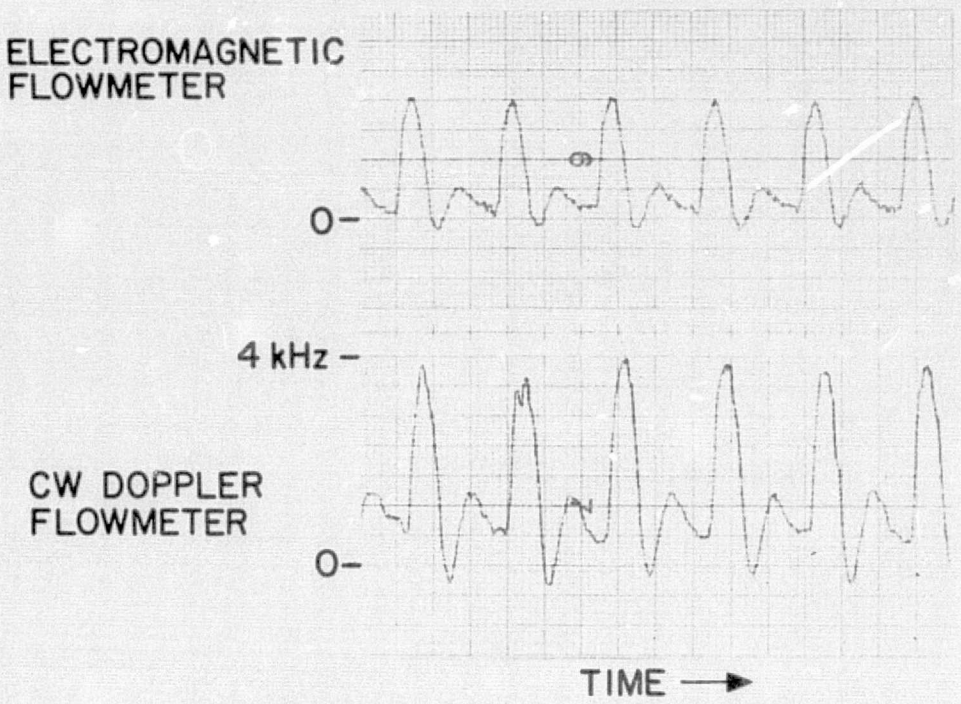


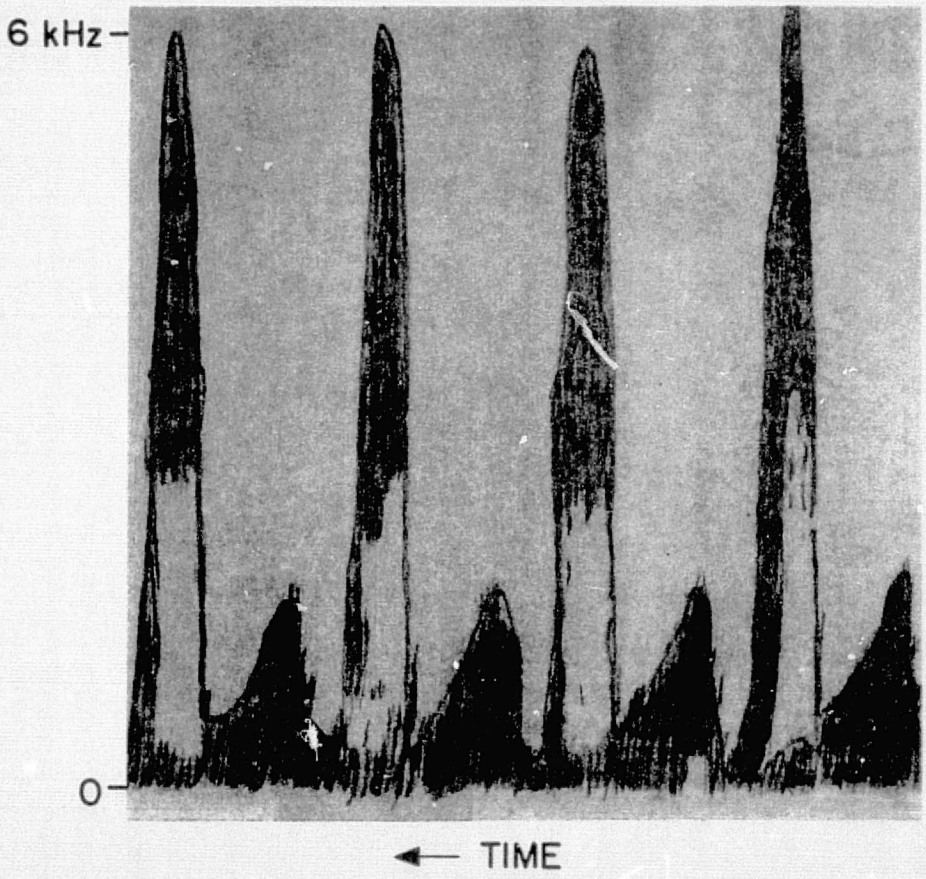


FIG 5.3 COMPARISONS BETWEEN FLOWMETER OUTPUT AND TIME VARYING DOPPLER SPECTRA (ACUTE CAL DATA)

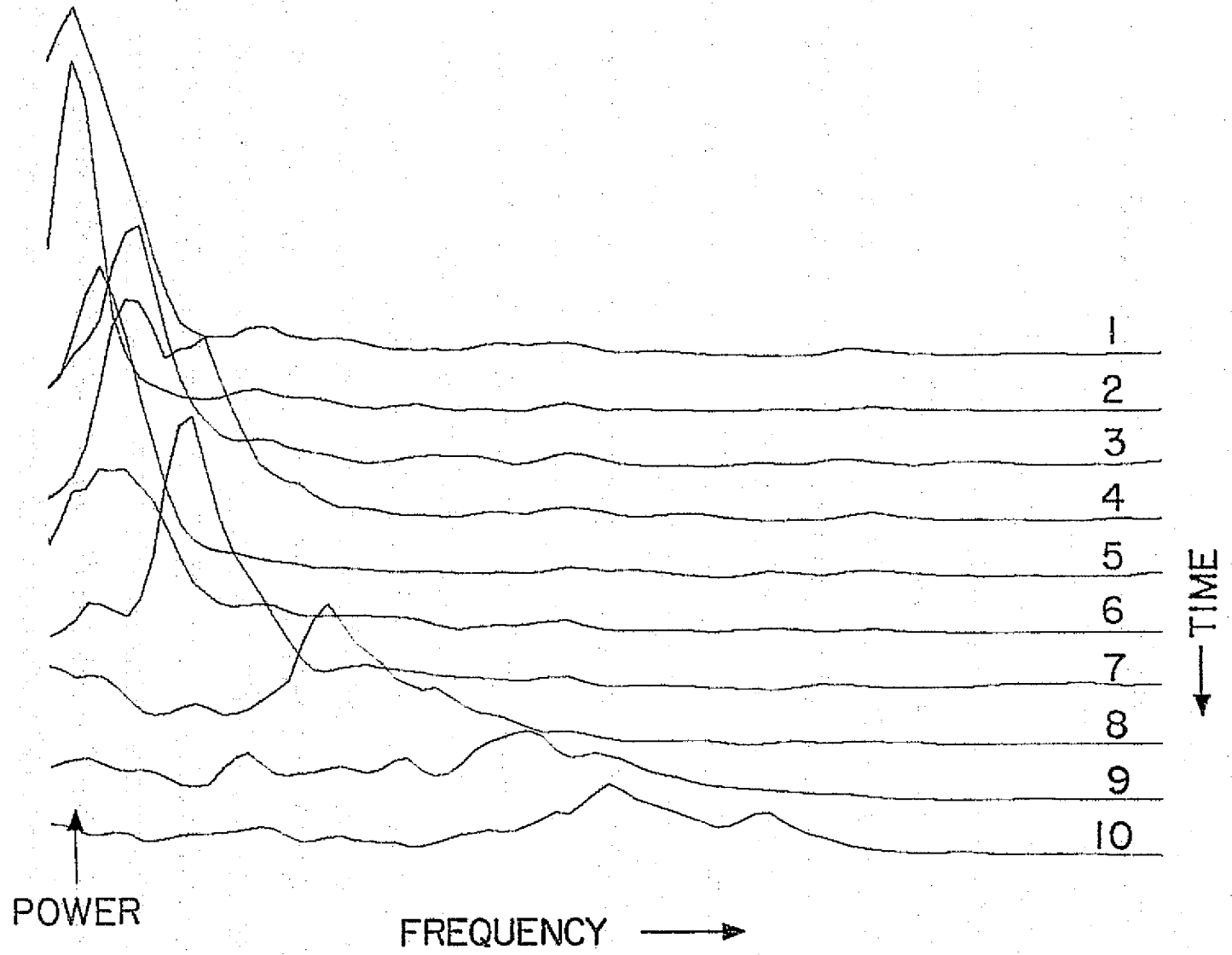


FIG 5.4 TIME VARYING DOPPLER SPECTRA DURING EARLY SYSTOLIC FLOW THROUGH THE DOG ILIAC ARTERY

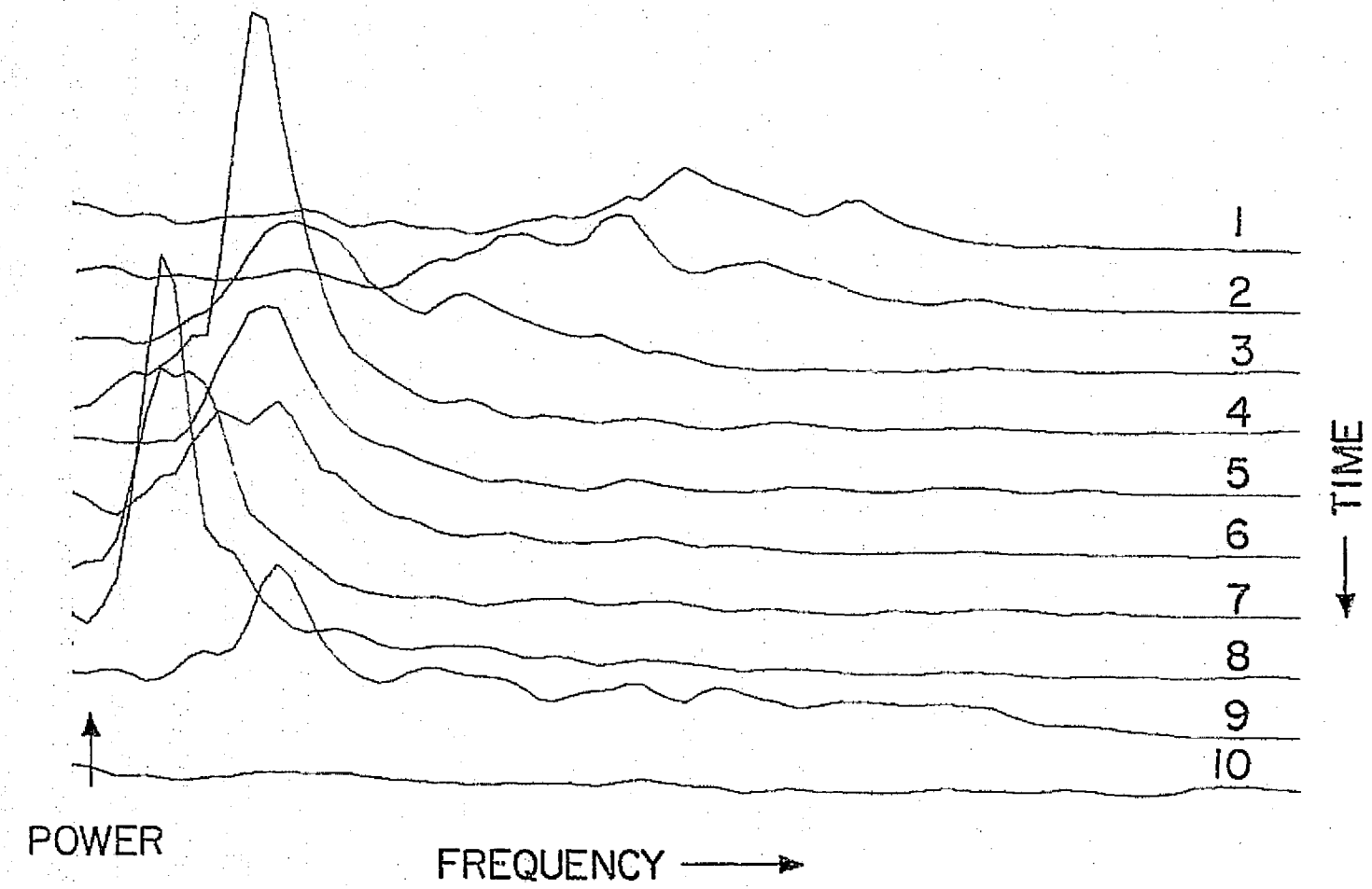


FIG 5.5 TIME VARYING DOPPLER SPECTRA DURING LATE SYSTOLIC FLOW THROUGH THE DOG ILIAC ARTERY

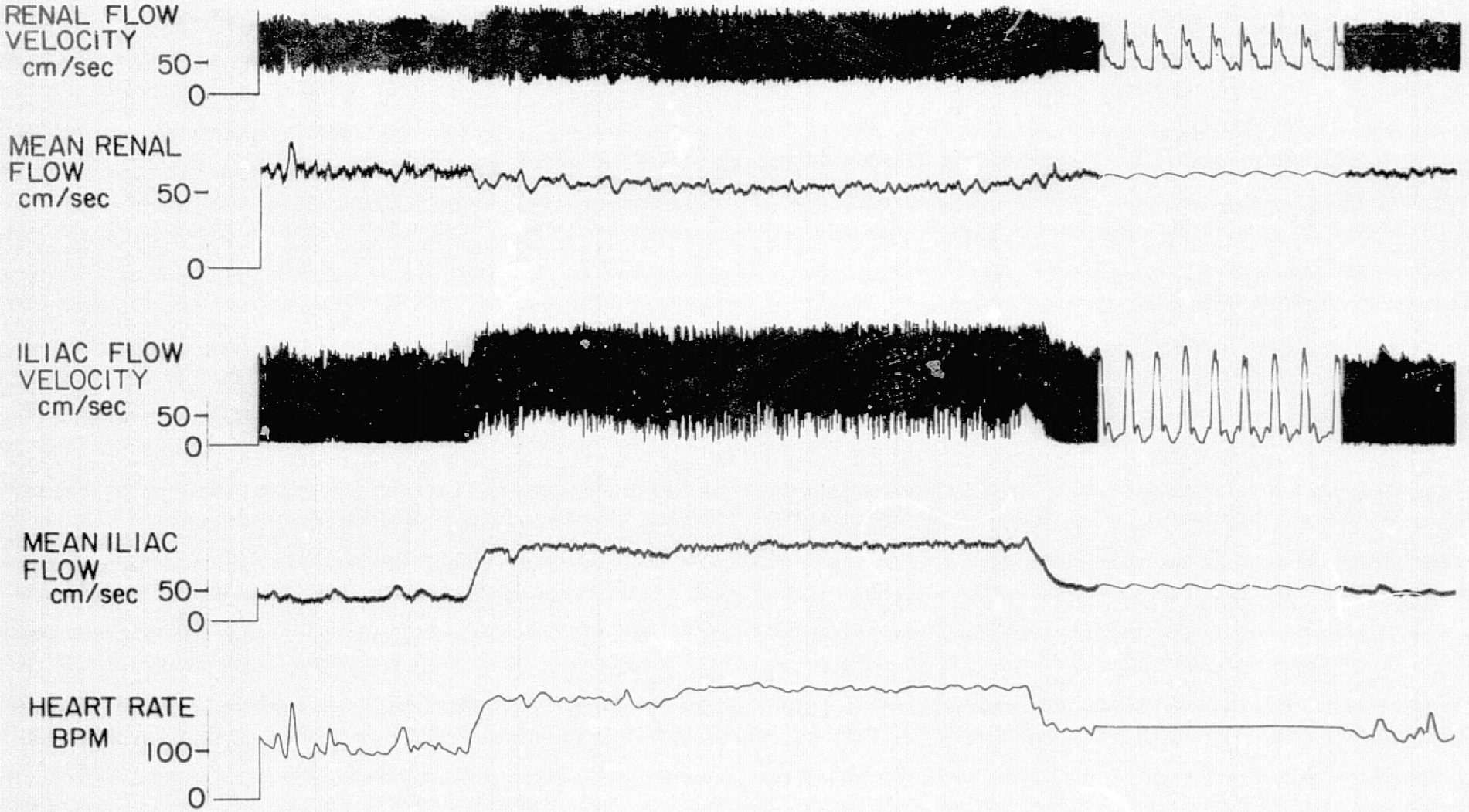


FIG 6.1 TELEMETERED FLOW DATA DURING REST, EXERCISE, AND RECOVERY

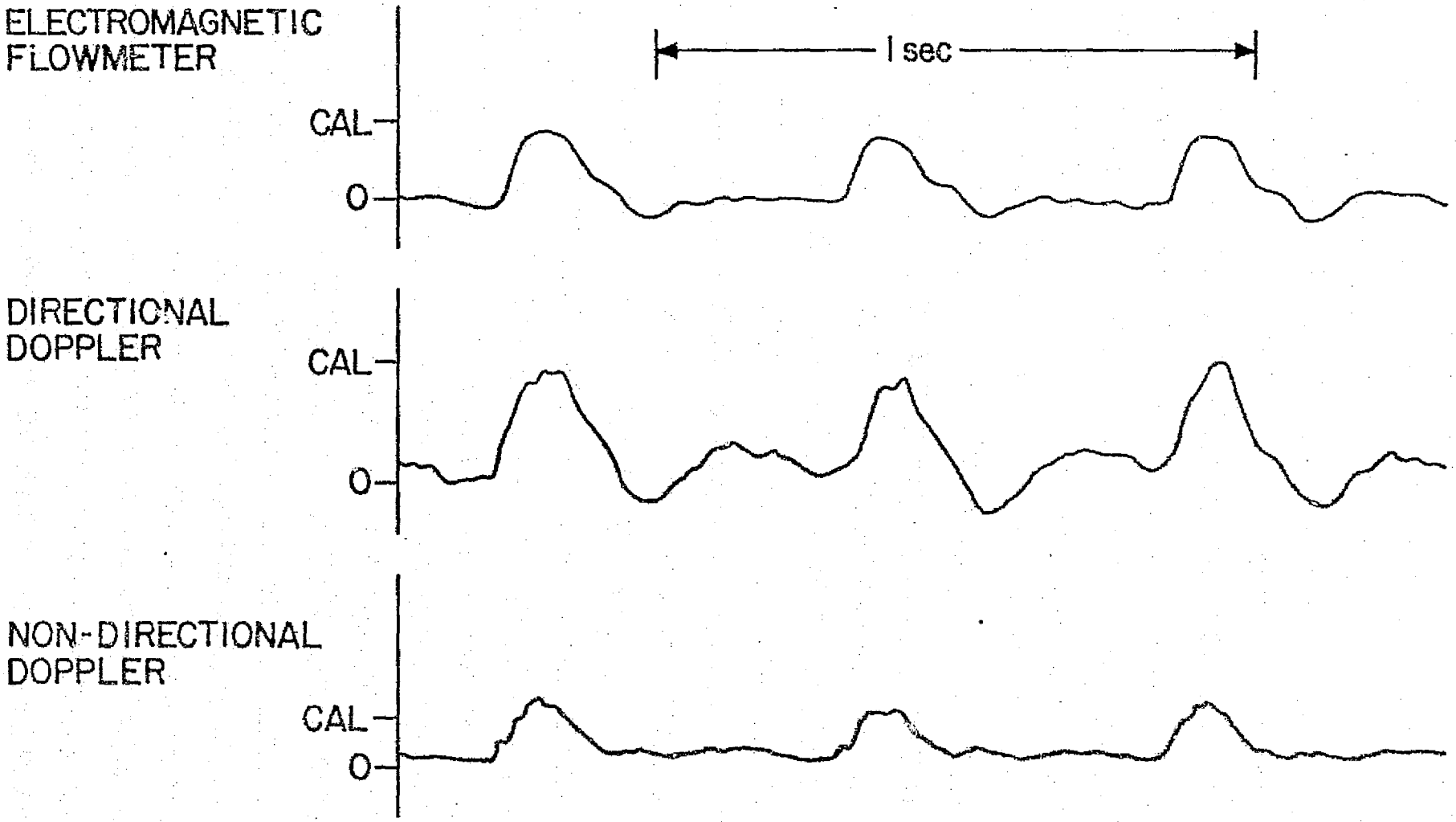


FIG 7.1 IMPLANTED PERFORMANCE OF DIRECTIONAL CW FLOWMETER

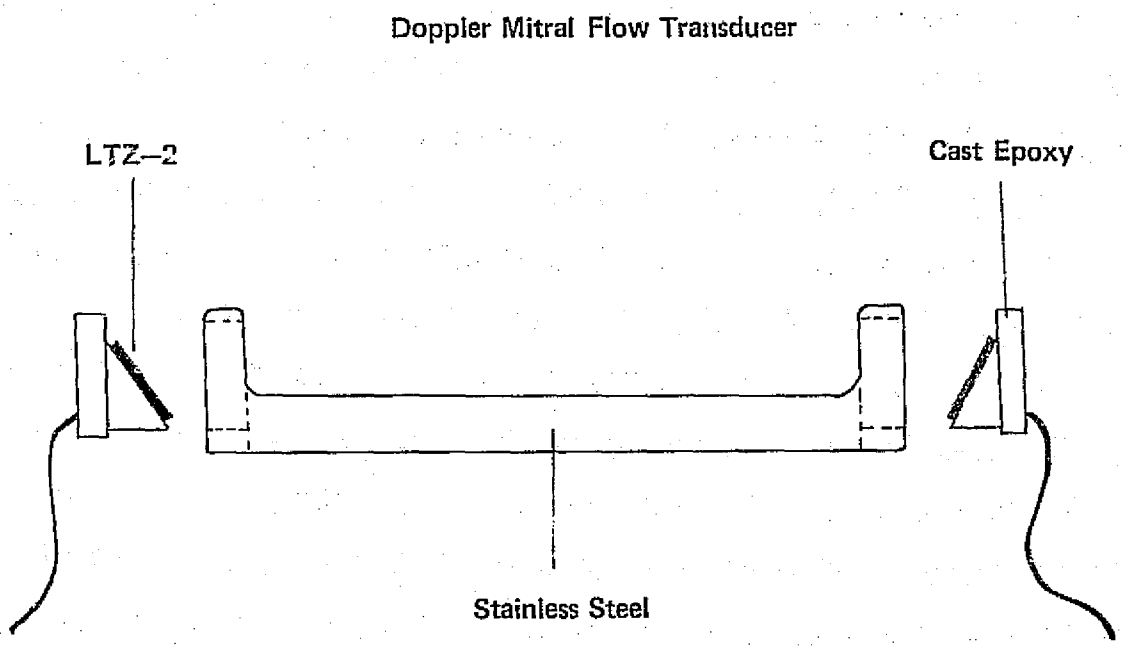


FIG 8.1 CONSTRUCTION DETAILS

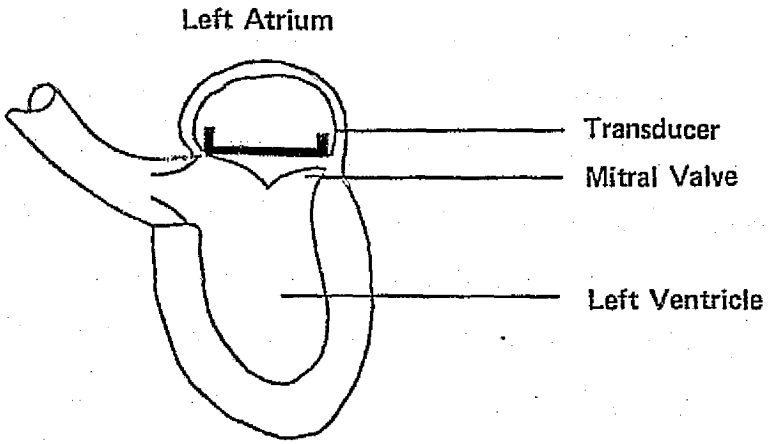


FIG 8.2 TRANSDUCER LOCATION

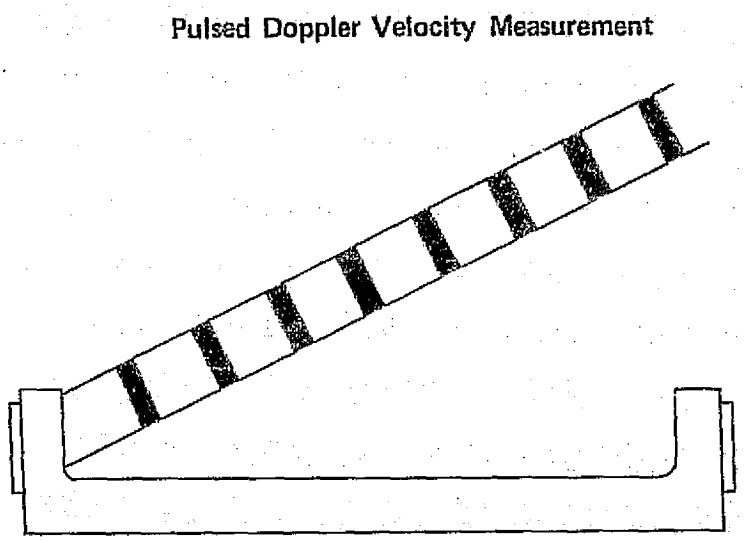


FIG 8.3 PULSED DOPPLER OPERATION

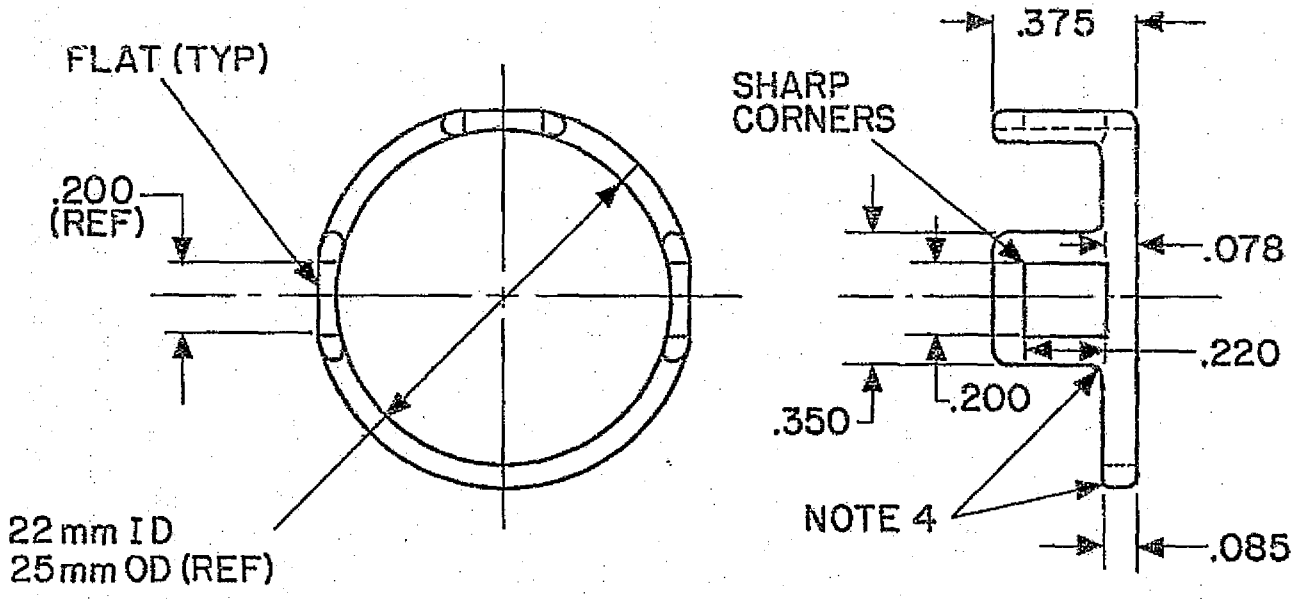


FIG 8.4 LOCATION OF TRANSDUCER ELEMENTS ON RING

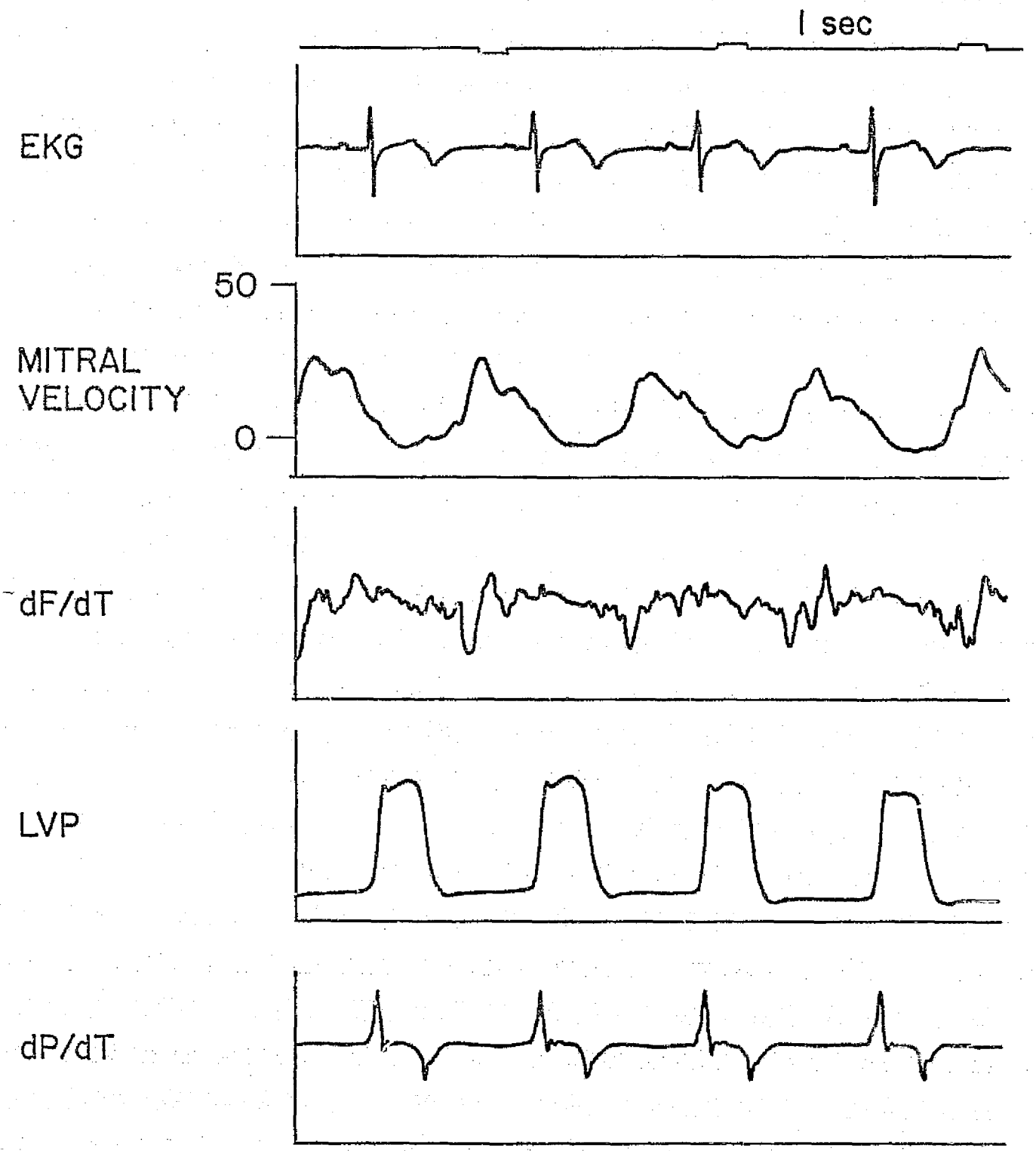


FIG 8.5 DATA COLLECTED DURING CW DOPPLER OPERATION

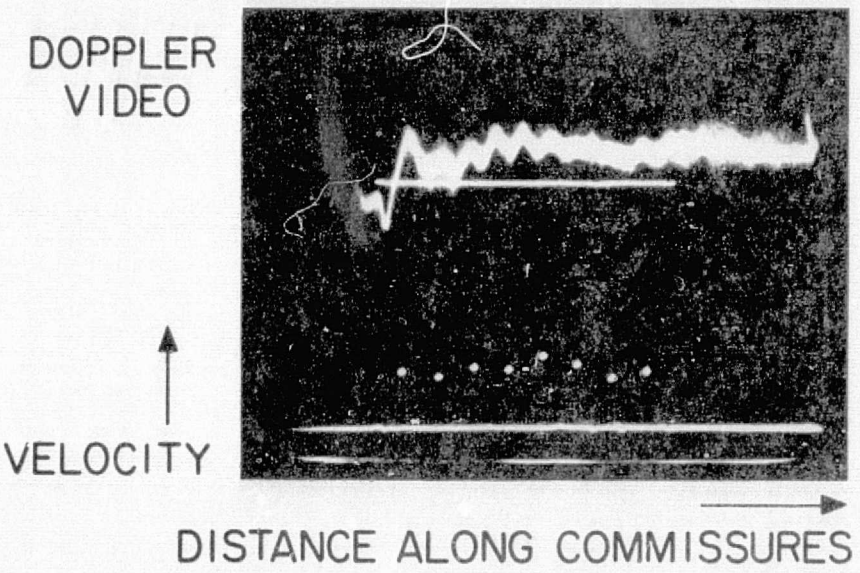


FIG 8.6 MEAN VELOCITY PROFILES ABOVE THE MITRAL VALVE

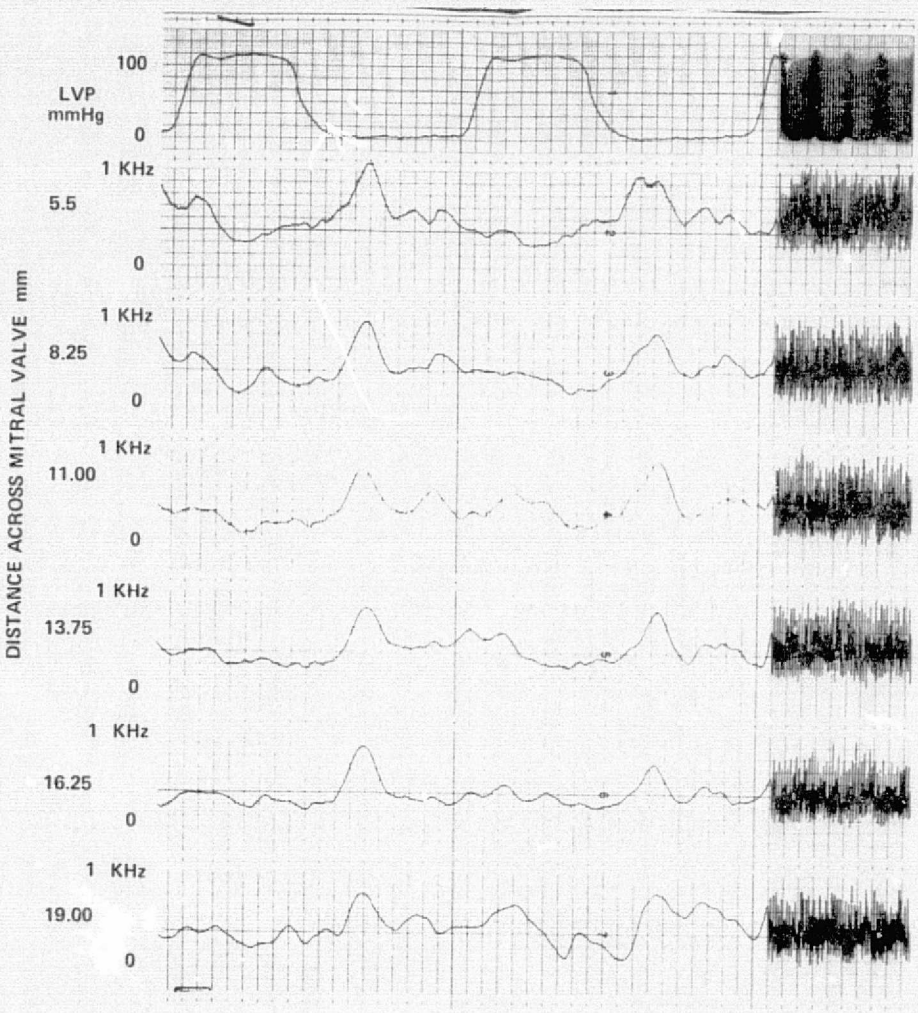


FIG 8.7 SIMULTANEOUS FLOW VELOCITIES ACROSS THE MITRAL VALVE

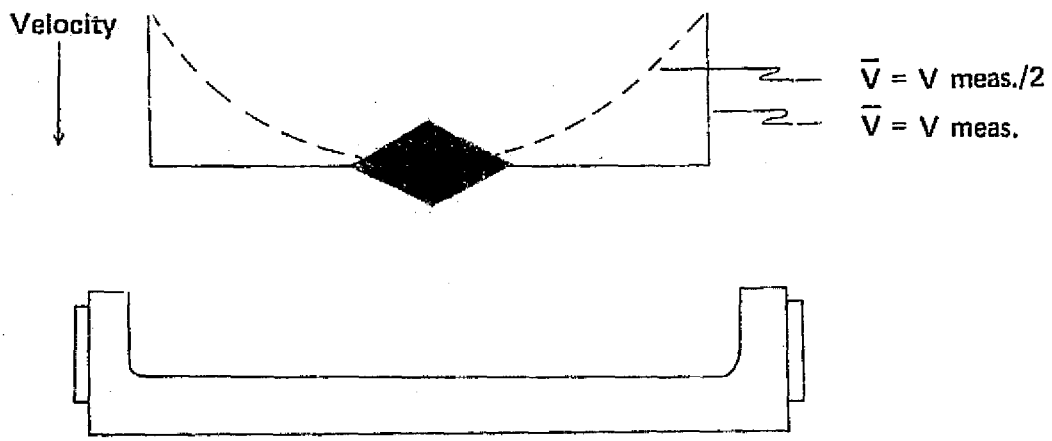


FIG 8.8 CW DOPPLER VELOCITY MEASUREMENT